



NTNU – Trondheim
Norwegian University of
Science and Technology

Power Electronics Converters for Microgrids with Smart Grid Functionality

Digital Implementation of Proportional
Resonant Controllers

Selie Galami

Master of Science in Electric Power Engineering

Submission date: June 2014

Supervisor: Lars Einar Norum, ELKRAFT

Co-supervisor: Roy Nilsen, Wartsilla

Norwegian University of Science and Technology
Department of Electric Power Engineering

Problem Description

Microgrids provide better reliability, lower losses and dynamic islanding among other traits. Dynamic islanding is one of the key features of a microgrid as it does not allow any negative or unwanted effects such as poor voltage quality to harm the local load sides at the microgrid end.

Traditional power grid approaches do not support renewable sources and distributed generation in an efficient way as microgrids. Hence, microgrid approach is deemed to be a suitable way to provide the rapid increment in power demand with both its dispatchable and standalone features.

Specifically, a different brand of controllers called Proportional Resonant controllers are to be studied in a microgrid setup along with other loop requirements such as virtual impedance and droop for better and stronger grid system in a continuous domain. The power sharing capability in multiple units and the system frequency are to be analyzed due to these controllers.

For laboratory implementation Proportional Resonant controllers are discretized and then their behaviour is analyzed both in MATLAB as well as laboratory environment.

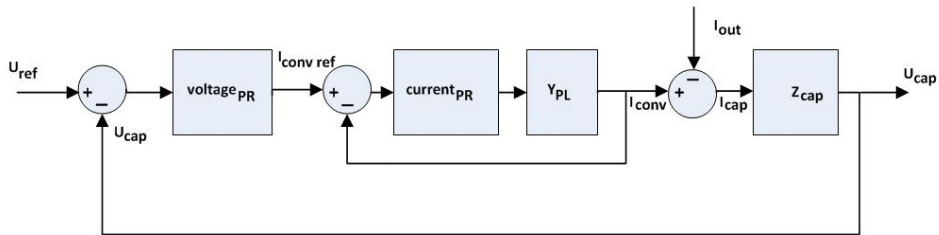
Abstract

The fast evolving technology has resulted in an extensive use of power electronics. The desire of making a grid network more intelligent can be fulfilled by these power electronics device. Based on the controller design and implementation, smartness feature can be improved. Real time communication requirement between the units in a grid can be removed by droop control.

The objective of this thesis is to do a thorough theoretical and practical study of Proportional Resonant controllers based on the journals available in the research field and then implement it in a digital setup, in order to realize its advantages over conventional Proportional Integral controllers.

All simulations were performed using the simulation software MATLAB Simulink. Additionally, another tool called OPAL-RT was used to interface discretized MATLAB Simulink models to the laboratory setup.

A preliminary test of Proportional Resonant controllers was done in continuous domain during Autumn 2013. It dealt with droop control for islanded operation mode (inductive output impedance) at different load conditions. The purpose of this preliminary project is to verify if the Proportional Resonant controllers can be implemented as voltage controllers for a single as well as multiple micrgrids in standalone operation mode. During this test, the current controllers were considered ideal. The system overview is shown in the figure below.



However, in order to investigate the effect of current controller in the overall system which includes the cascaded outer voltage controller, a Proportional Resonant current controller has been implemented in this study.

In order to prove that the established controllers are feasible, laboratory tests were conducted, thus requiring discretization of the established controllers.

A review of different discretization methods was conducted. The most suitable one for the

Proportional Resonant controllers is analyzed further and used to discretize the controllers. Thereafter, they are tested in both MATLAB Simulink and laboratory environment via a prototype setup.

Simulation results show that the established Proportional Resonant controllers work as intended. The laboratory tests which use the discretized controllers prove that the proposed controllers work, with comparable results as the simulations predicted.

The controller behaviour was not optimal in terms of the settling time issue but the most relevant task of reference tracking has been achieved.

Preface

I would like to put forward my words of gratitude to my two supervisors Professor Lars Einar Norum, Norwegian Institute of Science and Technology (NTNU) and Professor Roy Nilsen, Wäertsillä for their experienced guidance and generous support despite their busy schedules. Whenever I had doubts over some theories or I suffered from bouts of lack of self confidence, their words of motivation helped me keep my focus and to work on.

I would like to extend my genuine gratitude towards Dr. Salvatore D'Arco and Dr. Jon A. Suul for providing me with their laboratory setup and guiding me through this final semester despite their busy schedule, with my thesis work. I am really thankful for their immense support and guidance.

I have to remember my friends at NTNU for reminding me that I am not the only one in this tough ride and giving me words of wisdom and moments of fun to cherish even in this hectic schedule of our semester.

I would like to acknowledge Kristiansen Baricuatro for his concern and support inspite of being busy with his own thesis. Thank you for your remarks and advices on this report layout and for being the kind, honest and funny person that you are and have always been.

Last but not the least, my family and friends back home in Nepal have been extremely supportive and understanding of my long working hours on this project and missing out on some skype and viber dates. I take this opportunity to thank them for being with me always.

Selie Galami
Trondheim, 16 June 2014

Contents

Problem Description	i
Abstract	iii
Preface	v
Table of Contents	vii
List of Tables	xi
List of Figures	xiii
Nomenclature	xv
1 Introduction	1
1.1 Background	1
1.2 Summary of Autumn Project	2
1.2.1 Simulation Results	2
1.2.2 Conclusion	6
1.3 Objectives	6
1.4 Scope of work	6
1.5 Limitations	6
1.6 Methodology and Work Plan	7
1.6.1 Simulation Work Plan	7
1.6.2 Laboratory Work Plan	7
1.7 Outline of Report	7
2 Theoretical Background	9
2.1 Microgrid	9
2.2 Distributed Generation	11
2.3 Distributed Storage	12
2.4 Smart Grid Functionality	12

CONTENTS

2.5	Converter Control System Technology	13
2.5.1	Voltage and Current Control Loops	13
2.6	PR(H) Controllers	13
2.6.1	PR Controller Tracking Theory	14
2.7	Droop Control	16
2.7.1	Primary Control	16
2.7.2	Secondary Control	18
2.8	Virtual Impedance	18
2.9	Discretization: Requirements and Techniques	21
2.9.1	Discretization Complexity	21
2.9.2	Discretization Techniques	22
2.9.3	Influence of Discretization on Roots Distribution	22
2.9.4	Implementation of the Discretization Method	24
2.10	MATLAB Simulink	27
2.11	OPAL-RT	27
3	Case Studies	29
3.1	PR Current Controller: MATLAB Model Case Study	29
3.2	PR Voltage Controller: MATLAB Model Case Study	31
3.3	SINTEF MATLAB Model Case Study	32
4	Controller Design	35
4.1	Design of PR Current Controller: MATLAB Model Case Study 1	35
4.1.1	Bode Plot Results	36
4.2	Design of PR Voltage Controller: MATLAB Model Case Study 2	41
4.2.1	Model Background	41
4.3	Design of PR Controllers: SINTEF MATLAB Model Case Study 3	44
4.3.1	Results for the Current Controller only	44
4.3.2	Results for the Voltage Controller Cascaded with Current Controller	47
4.3.3	Testing with Prototype Parameters	48
5	Laboratory Work	51
5.1	General Layout	51
5.1.1	Components used in the Laboratory Setup	52
5.2	Results	52
5.2.1	Test Outcomes of a Current Controller	52
5.2.2	Test Outcomes of a Cascaded Voltage Controller with a Current Controller	55
6	Discussion	57
7	Conclusion	61
8	Future Work	63
	Bibliography	65

Appendix	69
A Simulink models	69
A.1 MATLAB Simulink Model for Parallel Two Units Standalone System . . .	69
A.1.1 Three Phase Current Supplied to the Load by the Two Parallel Units	72
A.1.2 Clarke Transformation	72
A.2 Detailed Connencions of the Masked Blocks for Figure 4.1 in Chapter 4 .	74
A.3 Stability and Tracking Analysis Results for Chapter 4	76
A.4 Pictorial Display of the Components used in the Laboratory Setup	80
A.5 MATLAB Coding	84
B Attached Files	89

CONTENTS

List of Tables

2.1	Test Values	26
3.1	Rated Values	30
3.2	Base Values	30
3.3	Base Values for the Circuit	32
3.4	Parameters for the Circuit	33
3.5	Rated Values for the Circuit	33

LIST OF TABLES

List of Figures

1.1	Frequency of the system for a resistive load of 20 kW.	3
1.2	Active power sharing between two units for a resistive load of 20 kW. . .	3
1.3	Reactive power sharing between two units for a resistive load of 20 kW. .	4
1.4	Frequency of the system for load switching.	4
1.5	Active power sharing between two units for load switching.	5
1.6	Reactive power sharing between two units for load switching.	5
2.1	Components of a microgrid.	10
2.2	Bode plot for a PR transfer function.	14
2.3	Open loop transfer function.	14
2.4	Closed loop transfer function.	15
2.5	Hierarchical control levels of a microgrid.	16
2.6	P-f and Q-U droop functions.	16
2.7	Synchronous Generator connection to the grid.	18
2.8	Closed loop controller strategy.	20
2.9	Output impedance in the system.	20
2.10	Virtual output impedance in the system.	21
2.11	Five groups of discretization techniques.	22
2.12	Block diagram of the discretized PR controller.	24
2.13	Simplified block diagram of inner current controller.	25
2.14	Reference tracking by the discretized current controller for h=1.	26
2.15	Reference tracking by the discretized current controller for h=1, 30, 40 and 50.	27
2.16	OPAL-RT features.	28
3.1	Single line diagram for the first case study of current controller only. . . .	29
3.2	Single line diagram for the second case study of current controller cascaded with voltage controller.	31
3.3	Single line diagram for the SINTEF MATLAB model case study.	32
4.1	MATLAB model for testing the discretized PR current controller.	36

LIST OF FIGURES

4.2	Closed loop tracking for case I for 50 Hz reference signal in alpha frame.	37
4.3	Closed loop tracking for case II for 50 Hz reference signal in alpha frame.	37
4.4	Closed loop tracking for case I for 50 Hz reference signal in beta frame.	38
4.5	Closed loop tracking for case II for 50 Hz reference signal in beta frame.	38
4.6	Closed loop tracking for case I for 100 Hz reference signal in alpha frame.	39
4.7	Closed loop tracking for case II for 100 Hz reference signal in alpha frame.	39
4.8	Closed loop tracking for case I for 100 Hz reference signal in beta frame.	40
4.9	Closed loop tracking for case II for 100 Hz reference signal in beta frame.	40
4.10	MATLAB model for testing the discretized PR voltage controller.	41
4.11	Closed loop of the voltage controller.	41
4.12	Closed loop of the voltage controller: simplified.	42
4.13	Bode plot closed loop tracking of voltage controller.	43
4.14	Scope result on voltage tracking.	43
4.15	Electrical setup in SINTEF MATLAB model for the current controller.	44
4.16	Closed loop current tracking for 50 Hz reference signal in alpha frame.	45
4.17	Closed loop current tracking for 50 Hz reference signal in beta frame.	45
4.18	Zoomed in look at the transient peak observation in beta frame.	46
4.19	Zoomed in look at the steady state observation in beta frame.	46
4.20	Working of the current controller for proportional and resonant gains of 1 and 1200 respectively in alpha frame.	47
4.21	Electrical setup in SINTEF MATLAB model for the voltage controller.	47
4.22	Working of the voltage controller.	48
4.23	Working of the current controller cascaded with a voltage controller.	48
4.24	Closed loop voltage tracking in alpha frame.	49
4.25	Closed loop current tracking in alpha frame.	49
4.26	Zoomed in view at the closed loop current tracking in alpha frame in steady state.	50
5.1	Schematic representation of the laboratory setup.	51
5.2	Transient response to the change in reference current.	53
5.3	Closer look at the three phase current waveforms.	53
5.4	Switching in each of the three phases of current.	54
5.5	Transient response to the change in reference voltage.	55
5.6	Closer look at the three phase voltage waveforms.	56

Nomenclature

Abbreviations

AC	Alternating Current	PI	Proportional Integral
CSI	Current Source Inverters	PLL	Phase Locked Loop
DC	Direct Current	PR	Proportional Resonant
DER	Distributed Energy Resources	PRH	Proportional Resonant Harmonic
DG	Distributed Generation	PV	PhotoVoltaic
DoE	Department of Energy	PWM	Pulse Width Modulation
DS	Distributed Storage	Q-U	Reactive power-Voltage
HIL	Hardware In the Loop	RL	Resistor-Inductor
LC	Inductor-Capacitor	SG	Synchronous Generator
NTNU	Norwegian Institute of Science and Technology	VSC	Voltage Source Converter
P-f	Active power-Frequency	VSI	Voltage Source Inverters
PCC	Point of Common Coupling	ZOH	Zero Order Hold

Symbols

Y_{PL}	admittance represented by the RL series circuit of the plant model	ϕ'_h	- phase angle of the plant function at the resonant frequency
z^{-1}	computational delay	θ	impedance angle
Z_{PL}	impedance represented by the RL series circuit of the plant model	E	voltage at the sending end
ϕ	voltage angle	G_{delay}	delay transfer function
ϕ'_h	delay compensation parameter	h	harmonic component
		h_o	voltage PR controller
		I_o	output current

NOMENCLATURE

k'_p	P-U droop	V	voltage at the receiving end
k'_q	Q-f droop	V_{cap}	capacitor voltage
K_{I_h}	resonant gain of the PR controller of the h harmonic component	V_{NL}	voltage at no load
K_{P_h}	proportional gain of the PR controller of the h harmonic component	V_{ref}	reference voltage
k_p	P-f droop	w	angular frequency
k_q	Q-U droop	w_1	fundamental angular frequency
L_f	filter inductance	w_{NL}	angular frequency at no load
P_L	active power at the given load	Z	line impedance magnitude
Q_L	reactive power at the given load	Z_c	capacitive branch impedance
R_f	filter resistance	Z_o	output impedance
T_s	sampling time	Z_v	virtual impedance

Introduction

1.1 Background

The rapid increase in power demand and the consumer need for better and reliable power quality has made the microgrid concept popular. Microgrid concept is not only applicable to those areas where the main grid cannot be taken or is too costly to be taken but with the smart grid functionality included in it, this can be extended to be used in either the grid interconnected operation or the standalone operation. These two different approaches to operation according to the situation demand plays a vital role to improve the reliability and quality of power at a reasonable cost thus, being a win-win situation for both the utility and the consumer ends.

Each microgrid features a converter with its own filter and different controllers for voltage and current parameters to be able to operate properly under any of the two schemes: grid interconnected and islanded (alone or in parallel with other microgrids).

The different controllers required by both the operational strategies described above can be:

- Proportional Integral (PI) controller
- Proportional Resonant (PR) controller

1.2 Summary of Autumn Project

The Autumn project dealt with the testing of a droop control PR voltage controller for islanded operation mode at different load conditions in a MATLAB simulink environment.

Following were the objectives of Autumn Project:

- Investigate cascaded control structure for standalone microgrid converter control consisting of an inner current control loop, outer voltage control loop and proper droop control.
- Design a robust current controller and voltage controller with PR controller.
- Implement Proportional Resonant Harmonic (PRH) controller controller for harmonic reduction at the microgrid (capacitor) and Point of Common Coupling (PCC) voltage.
- Implement and study parallel operation of microgrids in islanded mode.

The various controller studies and their parameter determination for the best result were first tried for the case of a single microgrid in a standalone system. Once a satisfactory result was obtained for this study case, parallel operation for microgrids still in islanded operation mode was studied. This study model in islanded case was further tested for different cases as:

- Load switching.
- Addition of a microgrid to the parallel (local) grid.
- Parallel operation of two or more microgrids.

After the islanded operation mode was successfully designed, synchronization technique was investigated to fully realize the smart grid functionality of microgrids with power converters as the title of the project stated.

1.2.1 Simulation Results

The results from the Synchronization study of multiple microgrids for an inductive output impedance with Active power-Frequency (P-f) and Reactive power-Voltage (Q-U) droops were not put in the Autumn report. These results have been now put in this Spring report under this section. The simulink model and many MATLAB blocks are placed at the appendix in the back from figures A.1 to A.5.

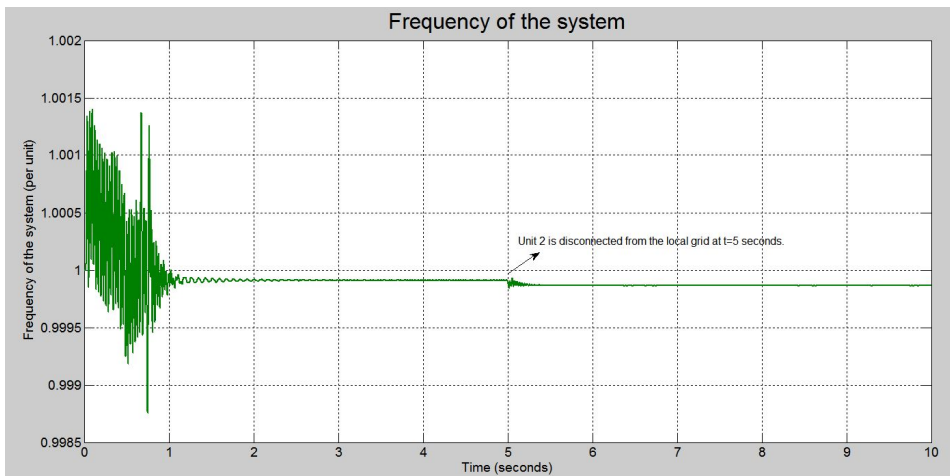


Figure 1.1: Frequency of the system for a resistive load of 20 kW.

Figures 1.1, 1.2 and 1.3 show the frequency of the system and the active and reactive power being shared between two units operating in islanded operation mode for a resistive load of 20 kW. Up to 3 seconds, unit 1 was feeding the resistive load but at 3 seconds, synchronization takes place such that the load now is being fed by both the units 1 and 2. Then, at 5 seconds, unit 1 is disconnected from the local grid and unit 2 feeds all the load. Since unit 1 has a lower P-f droop and a higher Q-U droop than unit 2, when both the units are in operation, unit 1 takes more active load than unit 2 as seen in the figure 1.2.

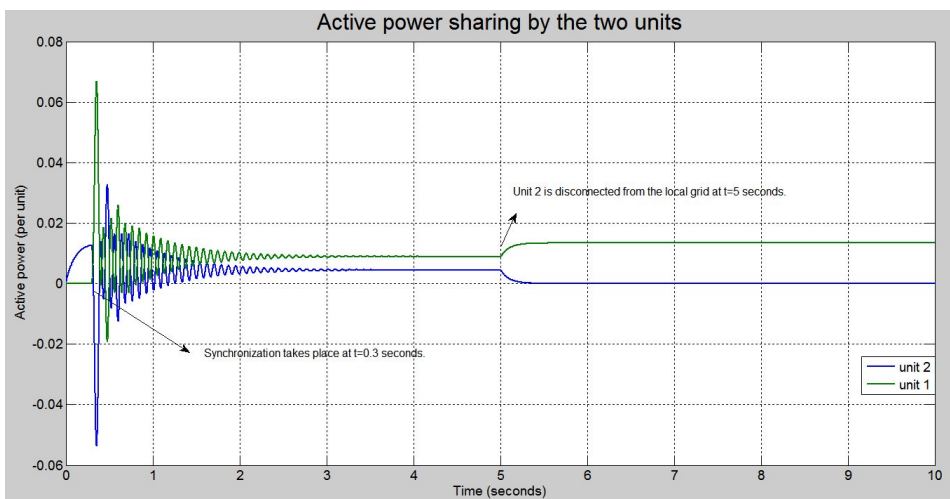


Figure 1.2: Active power sharing between two units for a resistive load of 20 kW.

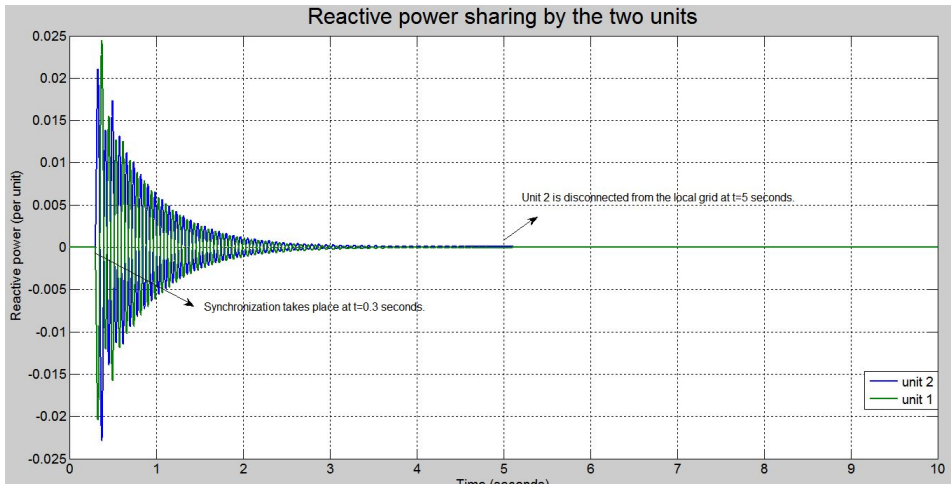


Figure 1.3: Reactive power sharing between two units for a resistive load of 20 kW.

The results for load switching were studied next. There are two sets of three phase balanced load: L1 (20 kW) and L2 (20 kW, 40 kVar). Unit 2 is initially feeding them. At t=0.3 s unit 1 is added to the existing system after synchronization. At t=2 s a three phase balanced load of 50 kW is added. At t=5 s unit 2 is disconnected from the local grid and the remaining load is fed by unit 1 only. At t=7 s load L2 is removed from the circuit. MATLAB simulation is run for 10 seconds to study the frequency and power feeds as shown in figures 1.4, 1.5 and 1.6.

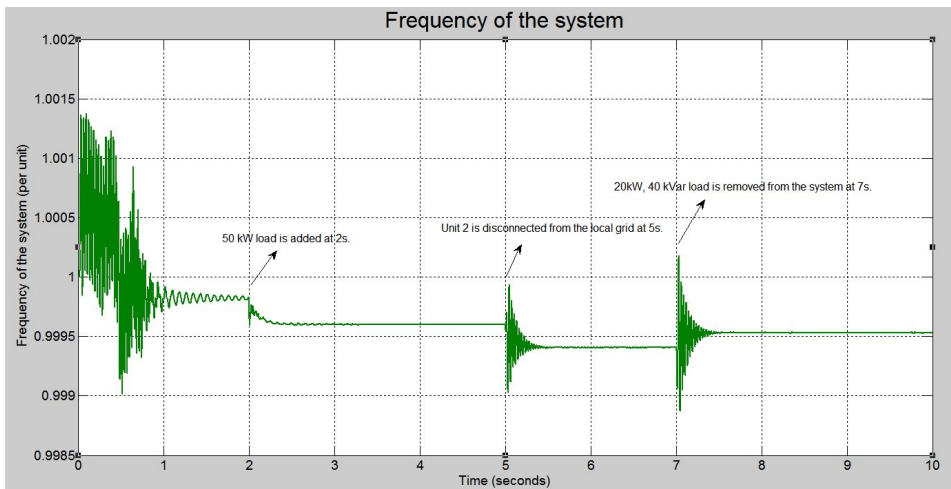


Figure 1.4: Frequency of the system for load switching.

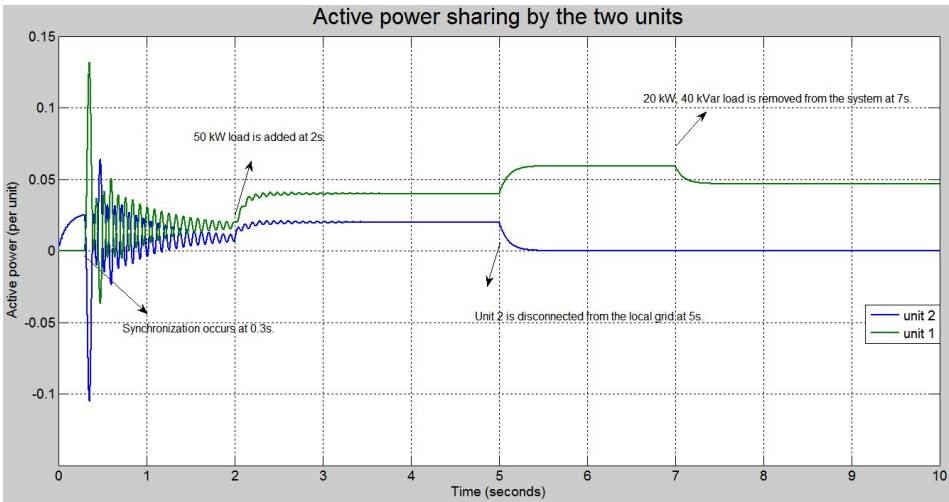


Figure 1.5: Active power sharing between two units for load switching.

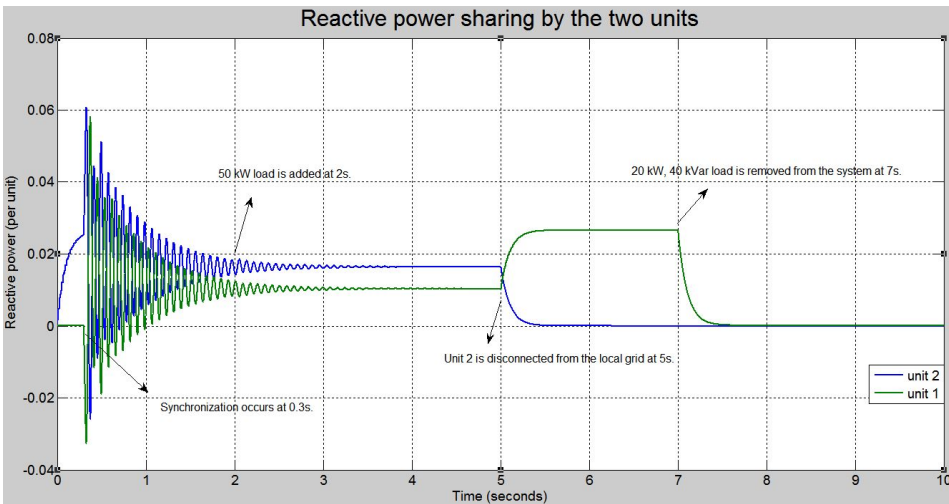


Figure 1.6: Reactive power sharing between two units for load switching.

As seen from the figure 1.4, the frequency of the system varies as per the load switching and the unit in operation as the units have different values of P-f and Q-U droops. At 2 seconds, with the addition of active load of 50 kW, the frequency of the system decreases because of the P-f relationship while further frequency drop is realized at 5 seconds with the disconnection of unit 2 because now unit 1 has increased active load. When the load of 20 kW and 40 kVar is removed at 7 seconds, frequency of the system increases because now, there is a decrease in the active power load seen by the remaining unit in the system. The figures in 1.5 and 1.6 show the same logic in the active and reactive power sharing between

the two units for the case of load switching and unit connection (synchronization) and disconnection (removal). The current supplied by the two units for this switched loading case is put in the appendix at the back from figures A.6 to A.7.

1.2.2 Conclusion

From the Autumn project the feasibility of PR voltage controller with droop control and virtual impedance implementation in a standalone operation of a single and multiple unit microgrid system was successfully carried out for different loads.

1.3 Objectives

Traditional power grid approaches do not support renewable sources and distributed generation in an efficient way as microgrids. Hence, microgrid approach is deemed to be a suitable way to provide the rapid increment in power demand with both its dispatchable and standalone features.

Specifically, a different brand of controllers called PR controllers are to be studied in a microgrid setup along with other loop requirements such as virtual impedance and droop for better and stronger grid system in a continuous domain. The power sharing capability in multiple units and the system frequency are to be analyzed due to these controllers.

For laboratory implementation PR controllers are discretized and then their behaviour is analyzed both in MATLAB as well as laboratory environment.

1.4 Scope of work

Following are the scope of work of this study:

- Investigate various discretization methods for the PR controllers.
- Implement the most optimal discretization technique on PR controllers.
- Design discretized PR current and voltage controllers.
- Test the discretized PR controllers in both MATLAB Simulink and a prototype setup.
- Identify potential improvement and strategy for future research work.

1.5 Limitations

Following are the limitations of this study, and will be done if time permits:

- Study of the discretized controllers with droop control schemes.

- Testing of the discretized controllers for different load types.

1.6 Methodology and Work Plan

After study of various literature study materials and the tutorial, Microgrids: Connecting Renewable Energy Sources into the Smart Grid by Josep M. Guerrero, Prof. Institute of Energy Technology, Aalborg University from EPE11 30 August to 1 September 2011, Birmingham, UK, the study model was created and simulation tools from MATLAB were implemented. Based on the working model in MATLAB Simulink, it is planned to be tested in a prototype at NTNU. Hence, basically, there are two work natures for this project. First, the simulation work and then the laboratory work.

1.6.1 Simulation Work Plan

MATLAB Simulink is used for the simulation part of the thesis study.

1.6.2 Laboratory Work Plan

After successful simulation of the system model, the analysis is then extended to a prototype test in a laboratory setup. OPAL-RT is used for the interfacing of discretized MATLAB Simulink models to the laboratory layout.

1.7 Outline of Report

In chapter 1, an introductory background about the thesis is given. It presents the summary of Autumn project as well as the objectives, limitations and the general approach and work plan to the thesis task. It provides an overview of the chapters to follow this introductory chapter as well.

In chapter 2, the different theories implemented on the project is reviewed. Concepts related to converter control to discretization and the tools used for either simulation task or laboratory implementation task have been put forward here.

In chapter 3, three case studies have been described for the analysis of discretization techniques and implementation on PR controllers. These case studies are all related to simulation analysis.

In chapter 4, design of PR controllers for each of the case studies is performed following the theoretical concept mentioned in chapter 2 and the results obtained are thoroughly analyzed and documented.

Chapter 1. Introduction

In chapter 5, the results from laboratory setup (final phase) for the current controller and the voltage controller designed in MATLAB are put forward. It discusses the results obtained from the laboratory setup.

In chapter 6, an overall discussion of the thesis along with discussions on individual case studies have been presented. It includes a comparative analysis on the simulation result and the laboratory result as well.

In chapter 7, individual conclusion from each of the case studies and an overall conclusion obtained from the project is given.

In chapter 8, further work that can be extended on this thesis project is commented.

Theoretical Background

This chapter gives a detailed documentation of the theories followed in the project.

2.1 Microgrid

A microgrid can be thought of as a small grid that can operate as a parallel part of a larger grid or operate independently from the larger grid. It is basically an electrical grid that can operate from its own power without a long distance transmission system or connection to a broader or main grid.

According to Department of Energy, United States of America (DoE), a microgrid is a group of interconnected loads and Distributed Energy Resources (DER) with clearly defined electrical boundaries that acts as a single controllable entity with respect to the grid [and can] connect and disconnect from the grid to enable it to operate in both grid connected or island mode. [1]

Each DER microgrid has the following components:

- Clustered DER units.
- Distributed Storage (DS).
- Converter.
- Loads.
- Interface switch.

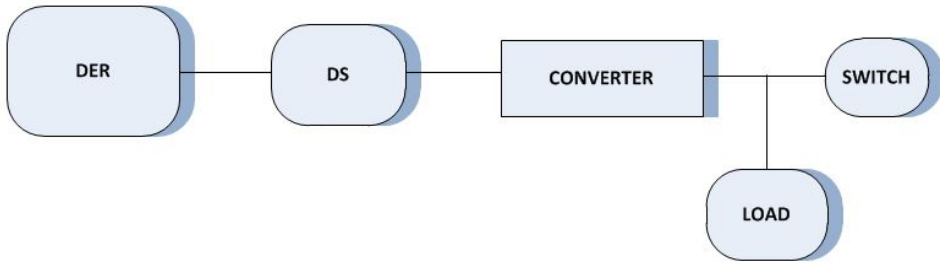


Figure 2.1: Components of a microgrid.

Figure 2.1 shows the different components of any microgrid. The interface switch allows it to act both as a dispatchable unit (as another grid source) when in closed position and a standalone unit (providing energy to local loads) when in open position unlike load or the main grid.

Microgrid Operation

With new and improved technologies at hand, industrial, commercial and residential consumers requirement for reliable and better quality of power has increased. The proposal of smart meters to meet these demands is complex and costly.

It is better to rely on multiple sources than a single one since the chances of an all-out failure is much less likely especially if extra generation is available. DER integrated microgrids with the decentralization of power supply can be an alternative to smart meters [2, 3]. In case of presence of more than one source, when there is an occurrence of system disturbances, planned island operation mode provides necessary power quality, availability and reliability to the consumers.

A number of DER integrated microgrids connected in parallel by an interface switch can be called a DER distribution system. This DER distribution system then operates in parallel connection to the main or central grid through an interface switch [2, 3].

Microgrid as a dispatchable unit

During this operation mode, the microgrid is in operation with a parallel connection to the main grid. It could be supplying power to the loads at the main grid or it could be supported by the main grid to partially or fully feed its local loads.

Microgrid as a standalone unit

In this operation mode, it is already disconnected from the main grid. This operation mode could be either preplanned or a result of system disturbance in the main grid.

The transition from the dispatchable unit behavior to the standalone unit behavior or vice versa is to be made as smooth as possible so that the system does not lose its stability. The different controllers for the microgrids play an important role in this part.

Microgrid Control System

When in standalone operation mode or an islanded operation mode, there is still a need that this microgrid system operates like a main grid system. Then, frequency control becomes a challenging problem. The frequency response for larger systems are based on inertia of rotating masses but for microgrids which are basically converter dominated grids without or with very small inertial rotating mass, this creates a problem. Hence, the control system for microgrid in standalone mode employs P-f droop to mimic inertial effect as that of large rotating masses, i.e. in an isolated microgrid, sources and loads coordinate via frequency [2, 4, 3].

For local reliability and stability, appropriate voltage regulation is also necessary. Voltage control requires that there is no large circulating reactive current between the sources. In the grid interconnected mode, this local problem of voltage control is mitigated by the Distributed Generation (DG) units as auxiliary local voltage support provider but in an isolated microgrid operation mode, it is realized by the Q-U droop controller implementation. These P-f droop and Q-U droop controllers employed in the control system of each microgrid generates the reference voltage for the system during standalone operation mode while during the grid interconnected mode, the main grid voltage itself is the reference voltage for the microgrid.

2.2 Distributed Generation

The high cost associated with the central or main grid for generation and transmission has resulted in many clustered generation and their associated loads, i.e. microgrids. Thus, with the increment in energy demand all around the world and the need for increased power reliability, microgrids have become extensively popular from economical, technological and environmental perspectives. Besides the conventional hydro plants and diesel generators, the many distributed renewable sources or the DG units such as PhotoVoltaic (PV), wind, fuel cells, microturbines are used in microgrid. This DER has lower emissions and an overall lower cost compared to the traditional ones.

The high voltage transmission network we have today is reliable and controllable but it suffers from cascading failures besides having poor efficiency and resource use. In fact central plants are best 35 % efficient because of line losses and smoke stack waste heat [2]. The distributed generation units in microgrids reduce the physical and electrical distance between generation and load side thus, providing: [2]

- Improved reliability
- Lower losses

- Enhanced voltage profile
- High penetration of renewable resources
- Dynamic islanding
- Distributed control and increased generation efficiencies through the use of waste heat
- Alternative to huge investments in new transmission and large scale generation systems

Dynamic islanding is a significant feature of a microgrid but all these objectives of a DER microgrid contribute to the realization of smart grid concepts and benefitting both the utility and the consumers.

2.3 Distributed Storage

Besides the distributed generation, microgrids also include DS for cases when generation and loads of the microgrid are not exactly matched. DS allows a way to fulfill the power and energy requirements at the microgrid. It allows DG units to run at a constant and stable output despite the load fluctuations. It also provides a ride through capability when there are dynamic variations of primary energy as solar, wind and hydro power sources and lets DG to seamlessly operate as a dispatchable unit. Most importantly it allows for storing energy for future demand.

Batteries, supercapacitors and flywheels are some examples of distribution storage in microgrids. Batteries are Direct Current (DC) power systems that require power electronics to convert the energy to and from the Alternating Current (AC) power. Often, bi-directional converters are used for both inflow and outflow of energy in the battery. Supercapacitors or ultra-capacitors are electrical energy storage devices offering high power density and extremely high cycling capability while flywheels, because of their fast response compared to electrochemical energy storage have now come into focus. [5, 6]

2.4 Smart Grid Functionality

DER smart grid functionalities are obtained by fast control of a number of individual units. This requires real time information on each of the DER units and key loads which just means control complexity. This control complexity is greatly reduced by the use of coupled DER integrated microgrids or parallel connected microgrids because: [2]

- A number of parallel connected microgrids do not need fast communication.
- Communication system of any kind re-dispatches each microgrid without requiring detailed information on each DER units.

Microgrids can disconnect from the central grid during events such as faults or voltage collapses but they can also be disconnected intentionally when power quality from the main grid falls below certain standard such that at least the local loads receive good power quality. Hence, for coupled or parallel connected microgrids, the number of microgrids and the types of DER units are irrelevant.

A microgrid can respond to a request of load curtail by increasing its internal generation and/or turning off some of the non-critical loads. [2]

Hence, the smart grid functionality is achieved by this plug and play [2, 7, 3] concept of microgrids with the information from each micro grid on the range of real and reactive power available for supply at each of them.

2.5 Converter Control System Technology

Inverters can be classified as Current Source Inverters (CSI) and Voltage Source Inverters (VSI). CSI are commonly used for current injection to the grid while VSI are used to maintain voltage stability. When an islanded operation mode is concerned, VSI are conveniently applicable. VSI are connected to energy storage devices, fixing the frequency and voltage inside the microgrid without any external reference to stay synchronized [4, 8]. The strategy for a converter control system requires an innermost current control loop and an outer voltage control loop.

2.5.1 Voltage and Current Control Loops

Current control loop is the innermost loop while voltage control loop is the outer loop. The voltage control loop consists of the PR controller with the capacitor voltage tracking the reference voltage. The immediate output of the voltage controller is the reference current for the current control loop. The converter current is made to track this reference current so this current control loop also has a PR controller in it. The need of a sinusoidal or undistorted microgrid voltage or the capacitor voltage means a harmonics free capacitor current.

2.6 PR(H) Controllers

In order to remove Phase Locked Loop (PLL) requirement, the abc frame is converted to stationary alpha-beta frame. Now that in the stationary alpha-beta frame, the values are sinusoidal instead, so the usual PI controllers cannot be employed. For achieving the zero steady state error for AC reference quantities, PR controllers are employed. PR controllers when employed for harmonics signals are termed as PRH controllers.

PI controllers, in general, are unable to remove the low harmonics component due to

bandwidth limitation. To increase the bandwidth, a high proportional gain is required but then this results in system stability becoming a critical issue. PR controllers and PI controllers have much in common; the difference being in the way the integration action takes part. In a PR controller the integrator will only integrate frequencies very close to the resonant frequency and will not introduce stationary error or phase shift. [9, 10]

2.6.1 PR Controller Tracking Theory

The magnitude and phase bode plot for an ideal PR controller is as shown in figure 2.2. It gives a very high dB magnitude gain at the resonant frequency. This high dB magnitude gain can be assumed to be infinite.

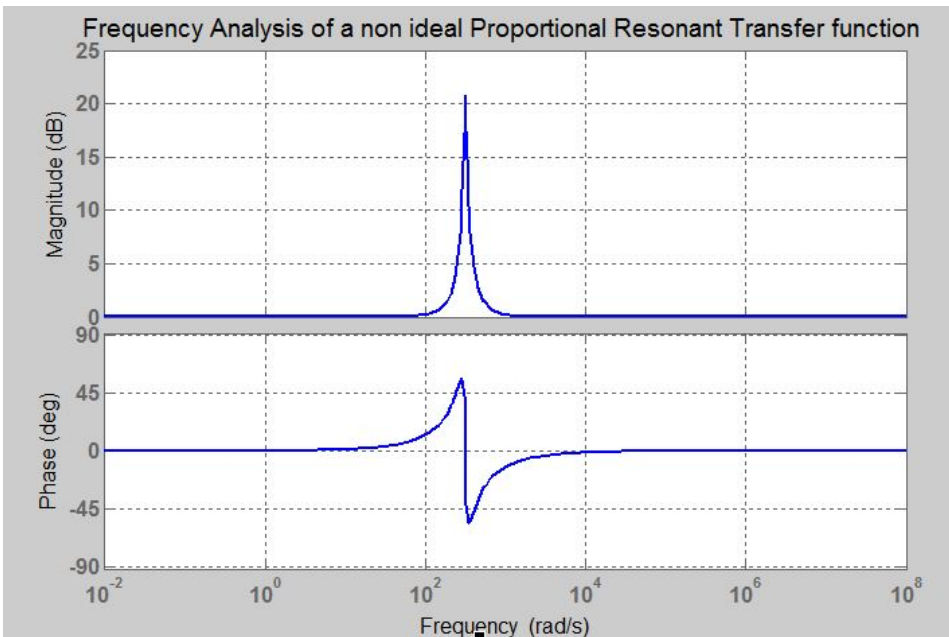


Figure 2.2: Bode plot for a PR transfer function.

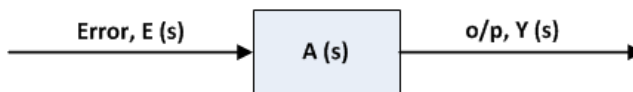


Figure 2.3: Open loop transfer function.

Figure 2.3 is the open loop transfer function for an ideal PR controller. The closed loop transfer function is as shown in figure 2.4.

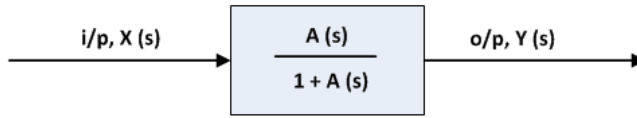


Figure 2.4: Closed loop transfer function.

For open loop case:

$$\frac{Y(s)}{E(s)} = A(s) \quad (2.1)$$

$$\text{magnitude } dB = 20\log|A(s)| \quad (2.2)$$

For $s = jw$

$$20\log|A(jw)|_{w=w_0} = \infty \quad (2.3)$$

$$\log|A(jw_0)| = \infty \quad (2.4)$$

$$|A(jw_0)| = 10^\infty = \infty \quad (2.5)$$

For closed loop case:

$$\frac{Y(s)}{X(s)} = \frac{A(s)}{1 + A(s)} \quad (2.6)$$

$$\text{magnitude } dB = 20\log \frac{|A(s)|}{\sqrt{1 + |A(s)|^2}} \quad (2.7)$$

For $s = jw_0$

$$\begin{aligned} \text{magnitude } dB &= 20\log \frac{|A(jw_0)|}{\sqrt{1 + |A(jw_0)|^2}} \\ &= 20\log \frac{\infty}{\infty} = 20\log 1 = 0 \text{ dB} \end{aligned} \quad (2.8)$$

So, for closed loop transfer function of an ideal PR controller the magnitude dB at the resonant frequency is 0 dB . This corresponds to a magnitude value of 1, i.e. the output response tracks the input value.

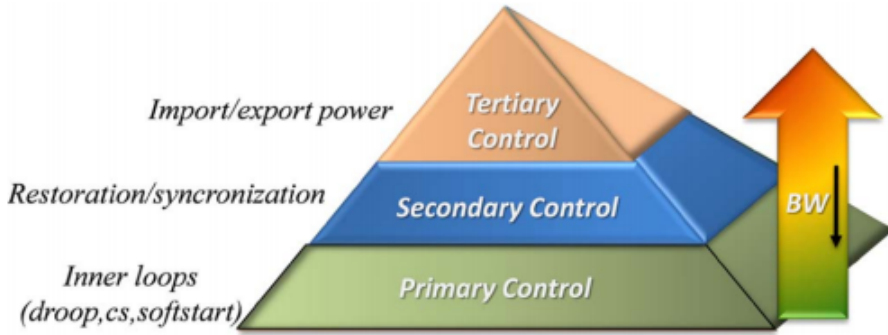


Figure 2.5: Hierarchical control levels of a microgrid. [4]

Following the control architecture in hierarchical manner, the most basic level for microgrid control as seen in figure 2.5 is the primary control as it provides reference to the voltage control loop so that the capacitor voltage tracks the reference voltage.

2.7 Droop Control

2.7.1 Primary Control

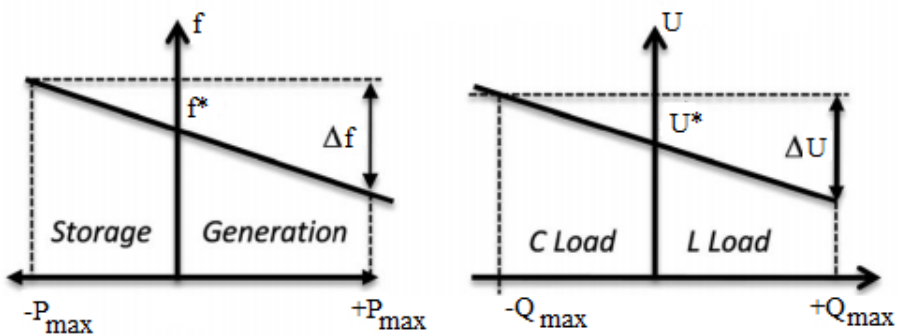


Figure 2.6: P-f and Q-U droop functions. [4]

Primary control is related to the stability of the electrical network. P-f droop and Q-U droop controls are implemented as primary controllers using a simple decentralized proportional

block [4]. The deviations introduced by the primary control are restored by centralized secondary control.

The droop primary control loop adjusts the reference voltage and frequency (reference voltage magnitude and angle, when speaking in terms of space vector) for the voltage controller loop. The droop primary controller loop mimics the actual P-f and Q-U droop relations for a Synchronous Generator (SG), thus providing the inertial action (inertial action is absent for active rectifiers) comparable to the SGs. So, following the droop concept, at steady state:

$$w = w_{NL} - k_p P_L \quad (2.9)$$

$$V = V_{NL} - k_q Q_L \quad (2.10)$$

where w is the angular frequency, w_{NL} and V_{NL} are the angular frequency and voltage at no load, P_L and Q_L are the active and reactive power at the given load while k_p and k_q are the P-f and Q-U droops respectively.

The above two relations are valid for an inductive impedance case while for a resistive impedance case, the two relations are modified to the relations given below:

$$w = w_{NL} + k'_q Q_L; \quad (2.11)$$

$$V = V_{NL} - k'_p P_L \quad (2.12)$$

where k'_q and k'_p are the Q-f and P-U droops respectively.

This role exchange of P and Q occurs because of the general formula for P and Q :

$$P = \frac{V}{Z} \{E \cos(\theta - \phi) - V \cos \theta\} \quad (2.13)$$

$$Q = \frac{V}{Z} \{E \sin(\theta - \phi) - V \sin \theta\} \quad (2.14)$$

where V and E are the voltages at the receiving and the sending ends respectively, Z is the line impedance magnitude while θ and ϕ are the impedance angle and the voltage angle respectively.

For an inductive impedance:

$$\theta = 90^\circ \text{ and } Z = X$$

while for a resistive impedance:

$$\theta = 0^\circ \text{ and } Z = R$$

Assuming ϕ to be very small such that $\cos \phi \approx 1$ and $\sin \phi \approx \phi$

For inductive impedance :

$$P = \frac{EV \sin \phi}{X} = \frac{EV\phi}{X}; \quad (2.15)$$

$$Q = \frac{EV(E - V)}{X} \quad (2.16)$$

For resistive impedance :

$$P = \frac{EV(E - V)}{R}; \quad (2.17)$$

$$Q = \frac{-EV \sin \phi}{R} = \frac{-EV\phi}{R} \quad (2.18)$$

2.7.2 Secondary Control

The deviation in frequency and voltage due to droop action can be eliminated by the implementation of a secondary controller. Secondary controllers are thus the frequency and amplitude restorers. The small change in frequency and voltage amplitude is given by: [4]

$$w = k_{pw}(w_{MG}^* - w_{MG}) + k_{iw} \int (w_{MG}^* - w_{MG})dt \quad (2.19)$$

$$E = k_{pE}(E_{MG}^* - E_{MG}) + k_{iE} \int (E_{MG}^* - E_{MG})dt \quad (2.20)$$

where k_{pw} and k_{pE} are the P-f and Q-U droops respectively while k_{iw} and k_{iE} are the integral P-f and Q-U droops respectively and MG stands for Micro Grid.

2.8 Virtual Impedance

The implementation of droop controller in the system was P-f and Q-U droop but this is not necessarily always correct. This was applied at the beginning as the islanded microgrid model was being emulated to the behavior of a synchronous generator.

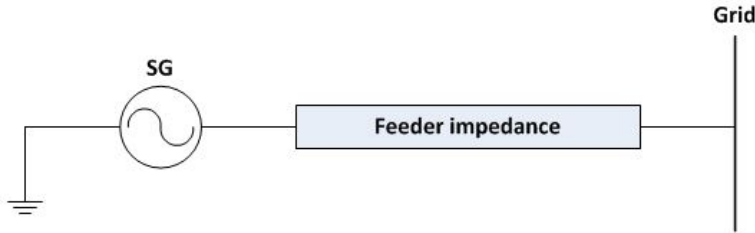


Figure 2.7: Synchronous Generator connection to the grid.

In figure 2.7, let the voltage at the SG be $E \angle \phi$ and that at the grid be $V \angle 0$. The feeder impedance is $Z \angle \theta$.

For a power flow from SG to the grid, the power equation is: [11]

$$\tilde{S} = \tilde{V} \times \frac{(E\angle -\phi) - V}{Z\angle -\theta} \quad (2.21)$$

$$\tilde{S} = \frac{V \times E \cos(\theta - \phi)}{Z} + j \frac{V \times E \sin(\theta - \phi)}{Z} - \frac{V^2 \cos \theta}{Z} - j \frac{V^2 \sin \theta}{Z} \quad (2.22)$$

$$P = \frac{V}{Z} \{E \cos(\theta - \phi) - V \cos \theta\} \quad (2.23)$$

$$Q = \frac{V}{Z} \{E \sin(\theta - \phi) - V \sin \theta\} \quad (2.24)$$

Generally for a SG, the line feeder impedance is assumed to be inductive, i.e.

$$Z = jX \text{ and } \theta = 90^\circ$$

Also, $\phi \approx 0$ or very small such that, $\sin \phi = \phi$ and $\cos \phi = 1$.

The angle ϕ is assumed to be zero, or matched with that of the main grid because this is the requirement for synchronization and this is achieved with the help of PLL.

Then,

$$P = \frac{EV}{X} \sin \phi = \frac{EV}{X} \phi \quad (2.25)$$

$$Q = \frac{V}{X} (E - V) \quad (2.26)$$

The above two relations show the active power and frequency proportional relationship as well as the reactive power and voltage change proportional relationship. For a SG, there exists a P-f and Q-U droop relationship and while implementing this characteristic for a microgrid inverter, the same droop controller scheme was implemented for voltage reference generation. As the inverter controllers are made so as to imitate the behavior of a SG, that imitation can be modified to incorporate good characteristics of a SG and enhance them for even better operation. The P-f, Q-U droop controllers indicate the impedance between the microgrid inverter and the LC filter output point has inductive output impedance. This is called a conventional droop method. However, for resistive output impedance, there are many advantages as: [12, 13, 14]

- The overall system is more damped.
- It provides automatic harmonic current sharing.
- Phase errors barely affect active power sharing.

Chapter 2. Theoretical Background

The output impedance of the inverter, unlike that of a SG, depends on the controller strategy and hence this output impedance of the inverter can be modified to become resistive in nature. This can be achieved by implementing virtual impedance via a control scheme on the already present output impedance from the controller strategy.

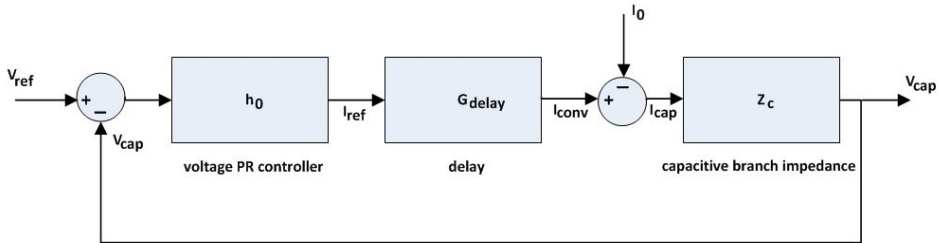


Figure 2.8: Closed loop controller strategy.

For the closed loop voltage controller illustrated in figure 2.8:

$$\{(V_{ref} - V_{cap})h_o G_{delay} - I_o\}Z_c = V_{cap} \quad (2.27)$$

$$V_{cap} = V_{ref} \left(\frac{h_o G_{delay} Z_c}{1 + h_o G_{delay} Z_c} \right) - I_o \frac{Z_c}{1 + h_o G_{delay} Z_c} \quad (2.28)$$

$$V_{cap} = G(s)V_{ref} - Z_o I_o \quad (2.29)$$

where V_{ref} is the reference voltage, V_{cap} is the capacitor voltage, h_o is the voltage PR controller, I_o is the output current, Z_c is the capacitive branch impedance and G_{delay} is the delay transfer function.

This corresponds to output impedance Z_o for the system as presented in figure 2.9.

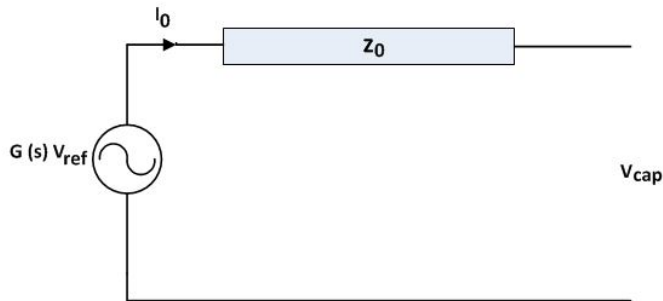


Figure 2.9: Output impedance in the system.

The transfer function Z_o is studied from its bode plot.

Let Z_v be the virtual impedance added such that, a simplified circuit looks as shown in figure 2.10:

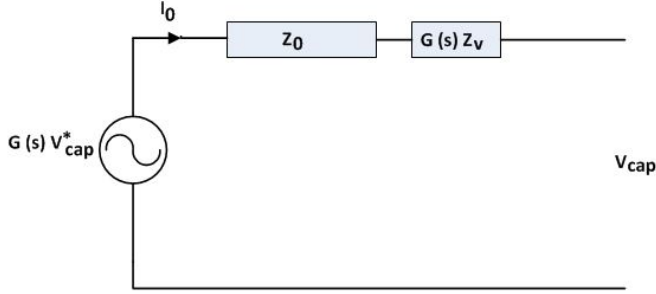


Figure 2.10: Virtual output impedance in the system.

In the controller viewpoint, the reference voltage is being modified [5, 15], such that:

$V_{ref} = V_{cap}^* - Z_v I_o$ is the no load voltage at the capacitor end. Then,

$$V_{cap} = G(s)(V_{cap}^* - Z_v I_o) - Z_o I_o \quad (2.30)$$

$$V_{cap} = G(s)V_{cap}^* - (Z_o + G(s)Z_v)I_o \quad (2.31)$$

Now, the modified output impedance is: $Z_o + G(s)Z_v$

2.9 Discretization: Requirements and Techniques

In order to have prototype analysis in a laboratory setup, it is recommended to have a detailed study in a discrete mode of the model.

2.9.1 Discretization Complexity

The change from continuous to a discrete mode is not an easy task as with the discretization implementation, there occurs displacement of poles which results in a deviation of frequency at which the infinite gain occurs with respect to the expected resonance frequency. [16, 17, 18, 19]

Discretization leads to a modification of zero distribution with respect to the continuous transfer function which affects stability of the system and, large values of resonant frequency have computational delays that affect system performance and may lead to instability [16, 17, 18, 19]. So, delay compensation has to be implemented [16, 17, 18, 19]. These delay compensation can be implemented in continuous domain but then, again the discretization process leads to a different expression from the actual one.

Hence, discretization implementation must be carried out with proper analysis.

2.9.2 Discretization Techniques

Based on the thesis and IEEE papers by Alejandro G. Yepes, the different discretization methods are discussed in terms of their implementation and similarity to the original continuous domain system and an optimal discretization method is defined as a concluding remark. The tabular figure 2.11 below has been taken from Yepes thesis and it shows the five groups of discretization techniques.

Group	Expressions ($i \in \{1, 2\}; j \in \{\text{PR}, \text{VPI}\}$)	Denominator
A	$R_{i_h}^f(z)$	$1 - 2z^{-1} + z^{-2}(h^2\omega_1^2T_s^2 + 1)$
B	$R_{i_h}^b(z)$	$(h^2\omega_1^2T_s^2 + 1) - 2z^{-1} + z^{-2}$
C	$R_{i_h}^t(z), G_{j_h}^{t\&t}(z)$	$(h^2\omega_1^2T_s^2 + 4) + z^{-1}(2h^2\omega_1^2T_s^2 - 8) + z^{-2}(h^2\omega_1^2T_s^2 + 4)$
D	$G_{j_h}^{f\&b}(z), G_{j_h}^{b\&b}(z)$	$1 + z^{-1}(h^2\omega_1^2T_s^2 - 2) + z^{-2}$
E	$R_{i_h}^{\text{zoh}}(z), R_{i_h}^{\text{foh}}(z), R_{i_h}^{\text{tp}}(z), R_{i_h}^{\text{zpm}}(z), R_{i_h}^{\text{imp}}(z)$	$1 - 2z^{-1}\cos(h\omega_1T_s) + z^{-2}$

Figure 2.11: Five groups of discretization techniques. [20]

In 2.11, the expression with R is the resonant part while the expression with G has both the proportional and resonant part. Also, R_1 and R_2 have the following expressions in s-domain. [20]

$$R_1(s) = \frac{s}{s^2 + h^2w_1^2} \quad (2.32)$$

$$R_2(s) = \frac{s^2}{s^2 + h^2w_1^2} \quad (2.33)$$

where h is the harmonic component and w_1 is the fundamental angular frequency.

2.9.3 Influence of Discretization on Roots Distribution

Resonant pole displacement [16, 17, 18, 19, 20]

Poles must be placed on the unit circumference corresponding to a zero damping factor or infinite gain. The damped resonant controllers do not assure perfect tracking. Resonant Groups C , D and E achieve infinite gain at the resonant frequency but for the same value of resonant frequency their poles are located at different positions of the unit circumference. Consequently, steady state error prevails. It is Group E whose implementation results in poles that match the original s-domain ones.

Zero distribution [16, 17, 18, 19, 20]

Infinite gain at the resonant frequency is given by pole placement whereas zeros only have a visible impact on the gain at other frequencies. Based on pole placement, Group E controllers are deemed the optimum type but then Group D controllers although causing a steady state error, save important resources by avoiding the calculation of explicit cosine functions when frequency adaptation is needed. In terms of delay compensation schemes, Group D controllers are not well suited.

So, first the infinite gain condition and then stability is verified for any implementation.

Between Group D and E resonant controllers there is a tradeoff between resource consumption when frequency adaptation is required and accuracy or selectivity (accurate peak position).

Keeping in mind the necessity for frequency adaptation, Group D resonant controllers are selected for discrete implementation. For pole placement, as mentioned earlier, Group E controllers are most suitable with their denominator:

$$1 - 2z^{-1} \cos(hw_1 T_s) + z^{-2} \quad (2.34)$$

where T_s is the sampling time. Group D controllers have the following denominator:

$$1 + z^{-1}(h^2 w_1^2 T_s^2) + z^{-2} \quad (2.35)$$

Group D controllers make use of two integrators system. For improving accuracy while using Group D controllers, their denominators can be improved to a higher order approximation such that: [16, 17, 18, 19, 20, 21]

$$(h^2 w_1^2) \rightarrow C_h = 2 \sum_{n=1}^{n_T/2} \frac{(-1)^{n+1} h^{2n} w_1^{2n} T_s^{2n-2}}{(2n)!} \quad (2.36)$$

From the impulse invariant discretization method,

$$G_{PR_h}^{dimp}(z) = K_{P_h} + K_{I_h} T_s \frac{\cos(\phi'_h) - z^{-1} \cos(\phi'_h - hw_1 T_s)}{1 - 2z^{-1} \cos(hw_1 T_s) + z^{-2}} \quad (2.37)$$

where K_{P_h} is the proportional gain and K_{I_h} is the resonant gain for the h harmonic component.

Equation 2.37 is a resonant controller from Group E , where ϕ'_h is a parameter to introduce delay compensation, the delay due to the plant function and the computational delays. This Group E resonant controller with delay compensation is very similar to that of a continuous domain representation.

The resonant controller with delay compensation and proposed corrections based on two integrators approach for frequency adaptation is given below in equation 2.38:

$$G_{PR_h}^d(z) = K_{P_h} + K_{I_h} T_s \frac{z^{-1} [\cos(\phi'_h) - hw_1 T_s \sin(\phi'_h)] - z^{-2} \cos(\phi'_h)}{1 - 2z^{-1} (1 - h^2 w_1^2 T_s^2 / 2) + z^{-2}} \quad (2.38)$$

$$hw_1 \sin(\phi'_h) \rightarrow \frac{1}{T_s} \cos(\phi'_h) - \frac{1}{T_s} \cos(hw_1 T_s \phi'_h) \quad (2.39)$$

Because of equation 2.39 and for each effect of additional z^{-1} delay, a phase corresponding to one sample delay of $hw_1 T_s$ is added to ϕ'_h such that $G_{PR_h}^d(z)$ now behaves similar to $G_{PR_h}^{dimp}(z)$. [20]

The block diagram for this discretization implementation of PR controller based on two integrators including resonant poles correction with delay compensation technique and accurate frequency adaptation is shown in figure 2.12:

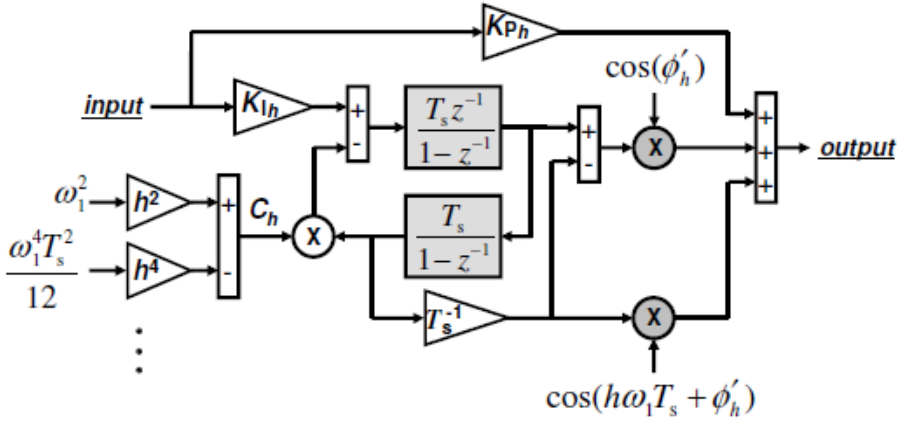


Figure 2.12: Block diagram of the discretized PR controller. [20]

Also, the final discrete PR controller expression is:

$$K_{P_h} + K_{I_h} T_s \frac{z^{-1} \cos(hw_1 T_s + \phi'_h) - z^{-2} \cos(\phi'_h)}{1 - 2z^{-1} (1 - C_h T_s^2 / 2) + z^{-2}} \quad (2.40)$$

2.9.4 Implementation of the Discretization Method

The selected discretization method is tested for the following simplified inner current controller in figure 2.13:

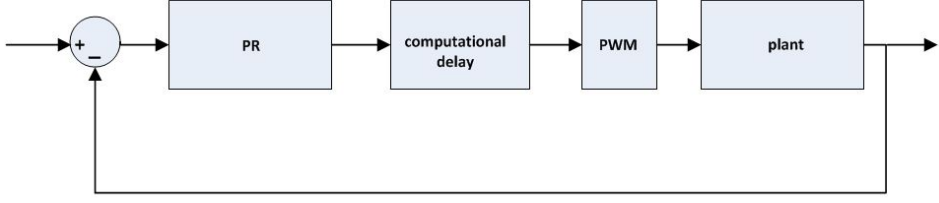


Figure 2.13: Simplified block diagram of inner current controller.

Plant modelling

The s-domain plant function is $G_f(s) = \frac{1}{sL_f + R_f}$ where R_f and L_f are resistance and inductance values of the filter. Considering the Pulse Width Modulation (PWM) operation of the converter, discretization is implemented by Zero Order Hold (ZOH) technique such that the plant model including the PWM effect is as shown in equation: [20]

$$G_f(s) = \frac{1}{sL_f + R_f} \xrightarrow{zoh} G_f(z) = \frac{1}{R_f} \frac{1 - e^{-\frac{R_f T_s}{L_f}}}{z - e^{-\frac{R_f T_s}{L_f}}} \quad (2.41)$$

The computational delay is represented by z^{-1} .

When implementing delay compensation, the value of the phase ϕ'_h should be such that the phase shift due to the plant function (including PWM and computational delay) should be compensated, hence:

$$\phi'_h = - \text{phase angle of the plant function at the resonant frequency [20]}$$

Based on these backgrounds, a discrete PR control was implemented from a proper continuous PR controller and the results on stability, accuracy and tracking characteristic were studied from bode plot as well as nyquist plot.

The discrete plant function including PWM and computational delay is given by equation 2.42 while the discrete PR current controller with all the corrections and delay compensation is shown in equation 2.43.

$$G_{PL}(z) = \frac{0.0199}{z^2 - 0.99z} \quad (2.42)$$

$$G_{cfb}(z) = \frac{0.08z^2 - 0.1597z + 0.07979}{z^2 - 1.999z + 1} \quad (2.43)$$

Chapter 2. Theoretical Background

For the following parameters:

Table 2.1: Test Values

Parameters	Values
harmonic component, h	1
Resonant angular frequency, ω_1	$2 * \pi * 50 \text{ rad/s}$
Proportional gain, K_P	0.08
Sampling time, T_s	0.0001 s
Filter resistance, R_f	0.5 Ω
Filter inductance, L_f	5 mH
Resonant integral gain, $K_I = K_P * R_f / L_f$	8

The bode plot stability analysis from nyquist plots are attached at the appendix while the system closed loop tracking for fundamental harmonic component and higher components, namely the 30th, 40th and 50th components are shown in figures 2.14 and 2.15.

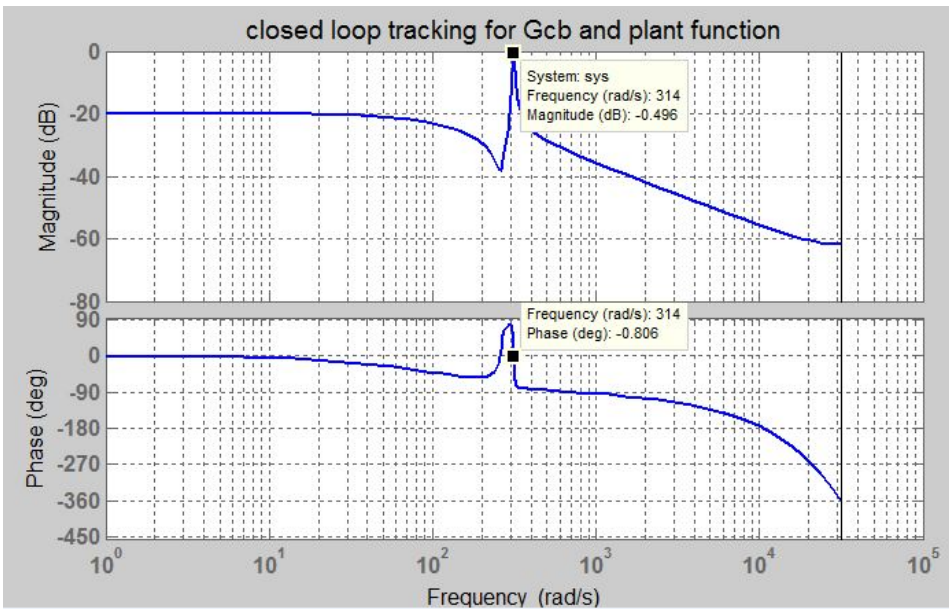


Figure 2.14: Reference tracking by the discretized current controller for $h=1$.



Figure 2.15: Reference tracking by the discretized current controller for $h=1, 30, 40$ and 50 .

2.10 MATLAB Simulink

In order to run models in a virtual scenario, MATLAB Simulink is one of the easy softwares available. It allows for model building as well as coding in m-file.

2.11 OPAL-RT

OPAL-RT provides a complete range of real-time digital simulators and control prototyping systems for power grids, power electronics, motor drives and other mechatronic systems. It offers powerful, scalable and affordable solutions for power systems and power electronics real-time simulation. [22]

These real-time systems help to perform feasibility studies, develop new concepts, design and test controllers for a wide variety of applications including small power converters, hybrid electric drives, large power grids and renewable energy systems. [22]

Laboratory implementations are realized by using RT-Lab Simulator. Based on studied theories a real-time PR controller has been realized and implemented on an OPAL-RT real time simulator. The physical converter and loads along with other required elements in the circuit are connected to the simulator and the whole set-up constitutes a Hardware In the Loop (HIL) system.



Figure 2.16: OPAL-RT features. [22]

Real-time simulator (Mx-Station) and its related equipments (probes and the PC unit), converter and loads were necessary to realize these tests. The HIL application demonstrates the reliability of such real-time simulators and effectiveness of active filters in a real physical application. Figure 2.16 shows the OPAL-RT features. [22]

Chapter 3

Case Studies

Before beginning with the laboratory work, the laboratory setup was tested in a virtual setup in MATLAB Simulink. There were two phases of MATLAB Simulink testing. First, analysis was performed for a simple model for both current and voltage controller: current controller only and current controller cascaded with a voltage controller. Thereafter, the study was extended to laboratory setup MATLAB Simulink model. Hence, overall there were basically three case studies performed.

3.1 PR Current Controller: MATLAB Model Case Study

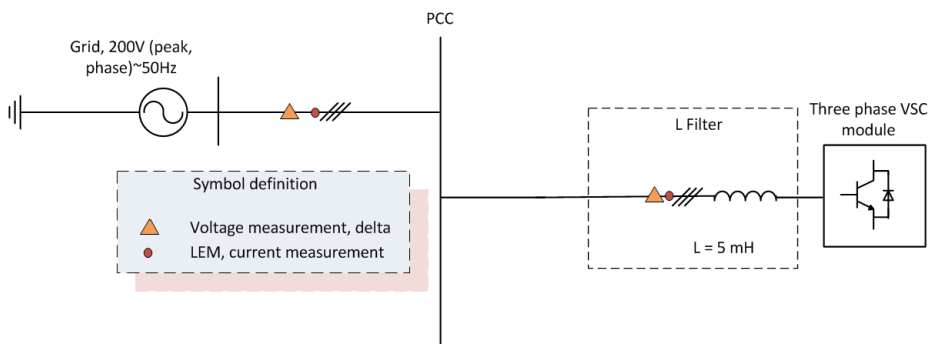


Figure 3.1: Single line diagram for the first case study of current controller only.

Figure 3.1 is a simple layout for the first case study regarding current controller only. A three phase Voltage Source Converter (VSC) module is connected to a grid through a Resistor-Inductor (RL) line and measurements are taken at the converter side as well as the

grid side for controller implementation to regulate the current being fed by the converter according to the reference values defined.

The tables 3.1 and 3.2 show the rated and base values used for case study 1 respectively.

Table 3.1: Rated Values

Parameters	Values
Rated apparent power, S_n	20 kVA (three phase)
Rated voltage, V_n	200 V (peak, phase voltage)
Rated current, I_n	66.667 A (peak phase current)
Rated DC voltage, V_{dc}	500 V
Rated frequency, f_n	50 Hz
Sampling time, T_s	200 μs

Table 3.2: Base Values

Parameters	Values
Base AC voltage, $V_{ac,base}$	V_n
Base AC current, $I_{ac,base}$	I_n
Base impedance, $Z_{ac,base}$	$V_{ac,base}/I_{ac,base}$
Base frequency, f_{base}	f_n
Base angular frequency, ω_{base}	$2*\pi*f_{base}$
Base resistance, R_{base}	$Z_{ac,base}$
Base capacitance, C_{base}	$Z_{ac,base}/\omega_{base}$
Base inductance, L_{base}	$Z_{ac,base}/\omega_{base}$

3.2 PR Voltage Controller: MATLAB Model Case Study

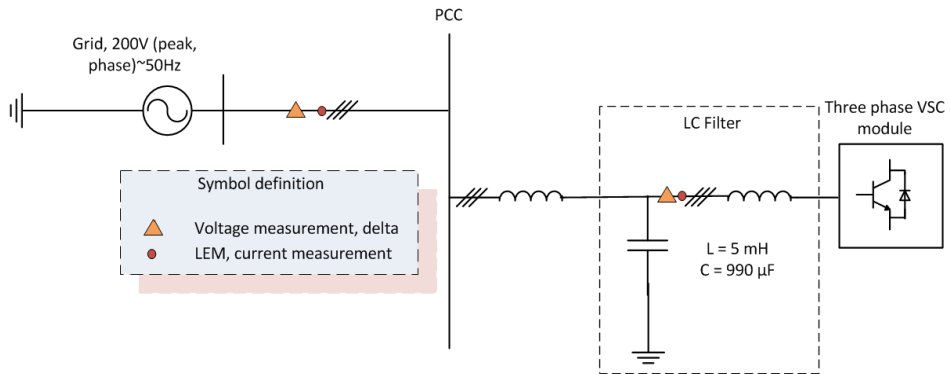


Figure 3.2: Single line diagram for the second case study of current controller cascaded with voltage controller.

Figure 3.2 is another simple layout for the second case study regarding current controller together with an outer voltage controller. A three phase VSC module is connected to a grid through a RL line with an Inductor-Capacitor (LC) filter and measurements are taken at the converter side as well as the grid side for controller implementation to regulate the current being fed by the converter according to the reference values obtained from the voltage controller that regulated the voltage across the capacitor according to the reference values defined for it.

3.3 SINTEF MATLAB Model Case Study

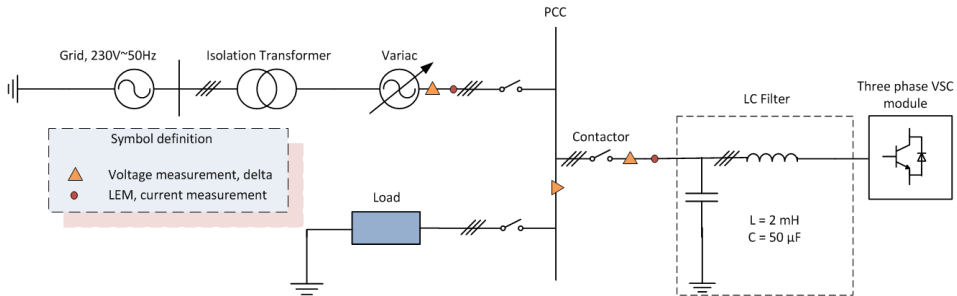


Figure 3.3: Single line diagram for the SINTEF MATLAB model case study.

Figure 3.3 shows the single line diagram for the SINTEF MATLAB model which depicts the laboratory setup model. Since only islanded operation model is studied, the contactor on the grid side is opened with the converter feeding the load only. The inductors are not ideal, that is, small resistances are also considered to be present as well.

The base, parameter and rated values of the circuit for this case study are as indicated in the tables 3.3, 3.4 and 3.5 respectively.

Table 3.3: Base Values for the Circuit

Parameters	Values
Base AC voltage, $V_{ac,base}$	326.5986 V
Base AC current, $I_{ac,base}$	102.0621 A
Base impedance, $Z_{ac,base}$	3.2000 Ω
Base frequency, f_{base}	50 Hz
Base angular frequency, w_{base}	314.1593 rad/s
Base resistance, R_{base}	3.2 Ω
Base capacitance, C_{base}	9.9472e - 04 F
Base inductance, L_{base}	0.0102 H
Base DC voltage, $V_{dc,base}$	653.1973 V

Table 3.3 shows the base values considered for the circuit.

Table 3.4: Parameters for the Circuit

Parameters	Values
Filter resistance, R_f	0.032 Ω
Filter inductance, L_f	0.002 H
Filter capacitance, C_f	50 μF
DC voltage, V_{dc}	2000 V

Tables 3.4 and 3.5 show the parameter and rated values considered for the circuit.

Table 3.5: Rated Values for the Circuit

Parameters	Values
Rated voltage, V_n	400 V (rms)
Rated current, I_n	72.1688 A (rms)
Rated frequency, f_n	50 Hz
Rated sampling time, T_{sc}	100 μs
Rated switching frequency, $f_{sw,ref}$	5000 Hz

Controller Design

For the controller design part, the approach followed is analysis and design for the first case study and thereafter, the second case study. Later, with these design experiences and ideas, design task is carried out for the third case study, thus finally completing the pre-laboratory tasks and then moving on to the prototype study.

4.1 Design of PR Current Controller: MATLAB Model Case Study 1

First, the desire is to look at the functioning of PR current controllers after discretization. Hence, a scope display is used to compare the reference current and the output current. A simple electrical system with a voltage source converter feeding an AC system through a transmission line is considered. The different components of this system are discussed below:

- Voltage source converter: An average-model based voltage source converter is used with a DC voltage source of 500 V.
- Transmission line: It is represented by a three phase series RL branch with a resistance of 0.5Ω and an inductance of 5 mH .
- AC voltage source: To be able to study the frequency variation effect, instead of a voltage source from the Simulink library, it is prepared differently with the frequency variation included as well. This can be found at the appendix in figure A.10.
- Current controller: PR current controllers are discretized according to the theories discussed in chapter 2. For the inclusion of frequency adaptation, the frequency input to the controller block is provided by a discrete PLL block. For analysis purpose only, the reference signal is provided by a Simulink library block called sine wave. To test

the success of the discretized PR current controller, the reference signal is tried as both a 50 Hz fundamental signal as well as a 100 Hz non-fundamental signal.

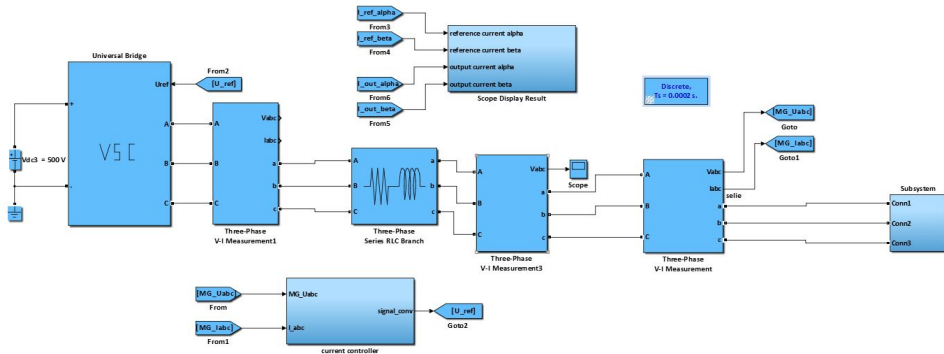


Figure 4.1: MATLAB model for testing the discretized PR current controller.

In the test MATLAB model in figure 4.1, the converter is represented by the VSC block which has a DC voltage supply of 500 V while measurements are taken from three phase V-I measurements. A three phase series RL branch depicts the transmission line (filter). Current controller block is masked whose detail layout is attached at the appendix under the section A.2. Similarly, the subsystem at the extreme right end masks the grid system whose detailed connection is attached at the appendix under the same section A.2. Other blocks as three phase voltage current measurement, mux, demux blocks from Simulink library are also used. Apart from those already available in the Simulink library, the need of abc to alpha-beta and vice versa is fulfilled by the use of defined equations existing between abc-alpha-beta in function blocks.

Besides the Simulink model, an m-file coding is also done to tune the best gain parameters of the defined discretized PR current controller taking into consideration all other requirements of stability and reference tracking. The simulation is carried out in discrete mode with Tustin as a solver type and a sampling time of 200 μs in powergui. The system is analyzed in per unit values and hence, the base values need to be defined. The rated values and base values are mentioned in tables 3.1 and 3.2 respectively.

4.1.1 Bode Plot Results

50 Hz as reference signal

For two cases, case I: proportional gain, $K_P=0.08$ and resonant gain, $K_I=25$ and case II: $K_P=1$ and $K_I=300$ the tracking response expected from frequency analysis as well as the scope results are shown in figures 4.2, 4.3, 4.4 and 4.5 while the nyquist and frequency stability plot and the frequency tracking plot are placed in the appendix under the section A.3 for both the sets of parameters.

4.1 Design of PR Current Controller: MATLAB Model Case Study 1

The slow magnitude tracking is dependent on the value of the gain parameter, K_I . The larger the value of K_I , the faster is the magnitude tracking. But then, it should be kept in mind that K_I should be tuned to obtain an adequate compromise between selective filtering and dynamic response.

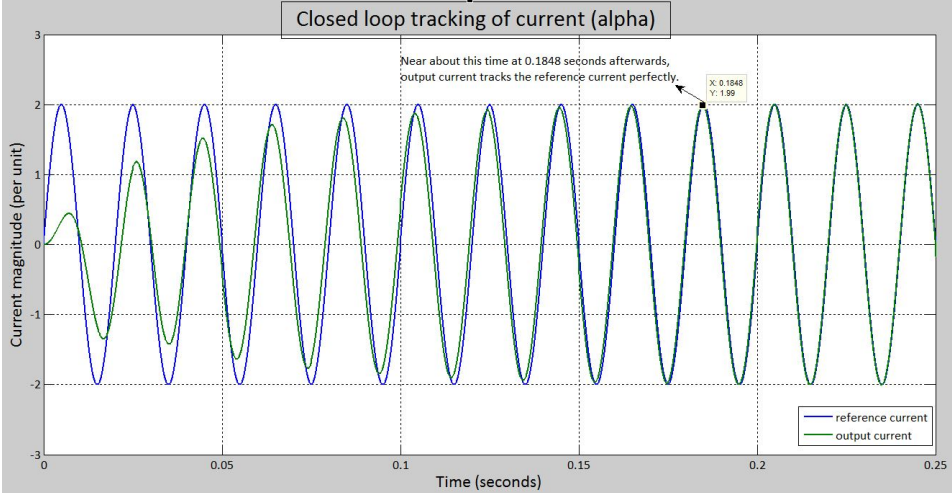


Figure 4.2: Closed loop tracking for case I for 50 Hz reference signal in alpha frame.

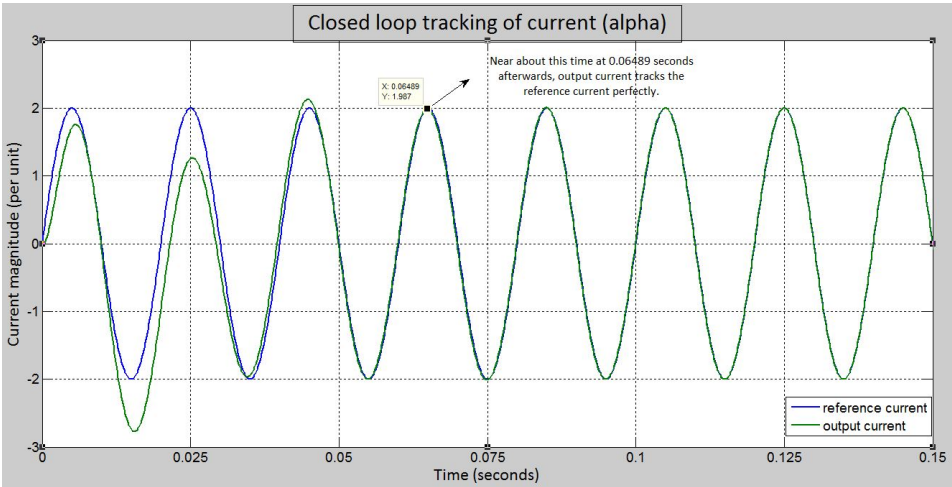


Figure 4.3: Closed loop tracking for case II for 50 Hz reference signal in alpha frame .

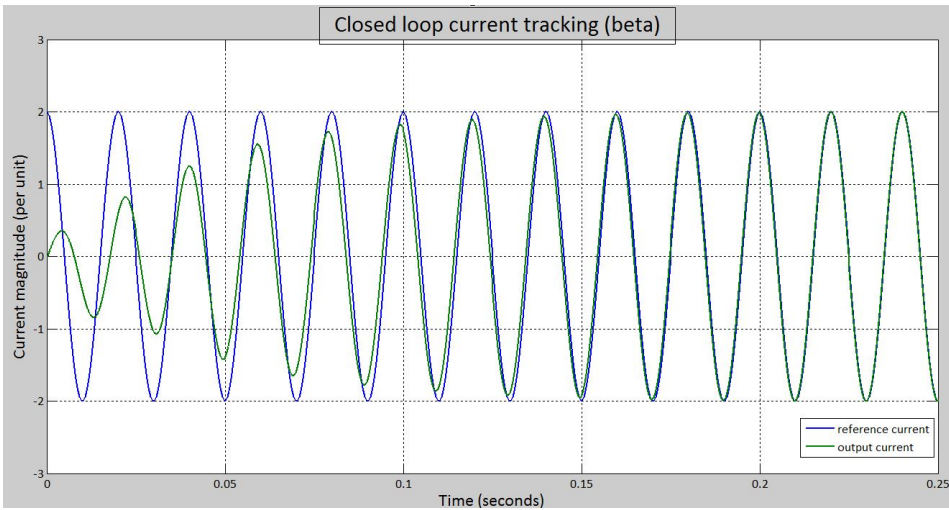


Figure 4.4: Closed loop tracking for case I for 50 Hz reference signal in beta frame .

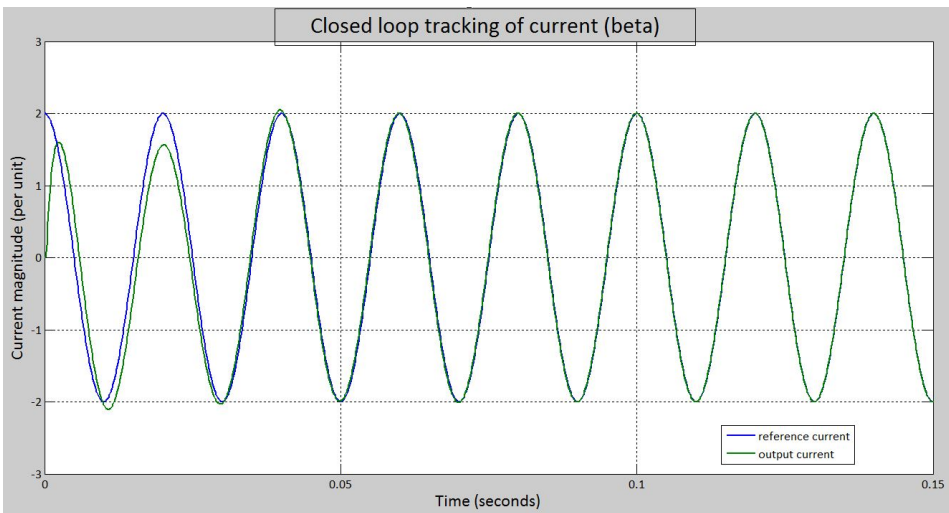


Figure 4.5: Closed loop tracking for case II for 50 Hz reference signal in beta frame .

100 Hz as reference signal

For the same two cases, case I: $K_P=0.08$ and $K_I=25$ and case II: $K_P=1$ and $K_I=300$ the tracking response expected from frequency analysis as well as the scope results are shown in figures 4.6, 4.7, 4.8 and 4.9. The rejection nature for frequencies other than the resonant frequency is being tested.

4.1 Design of PR Current Controller: MATLAB Model Case Study 1

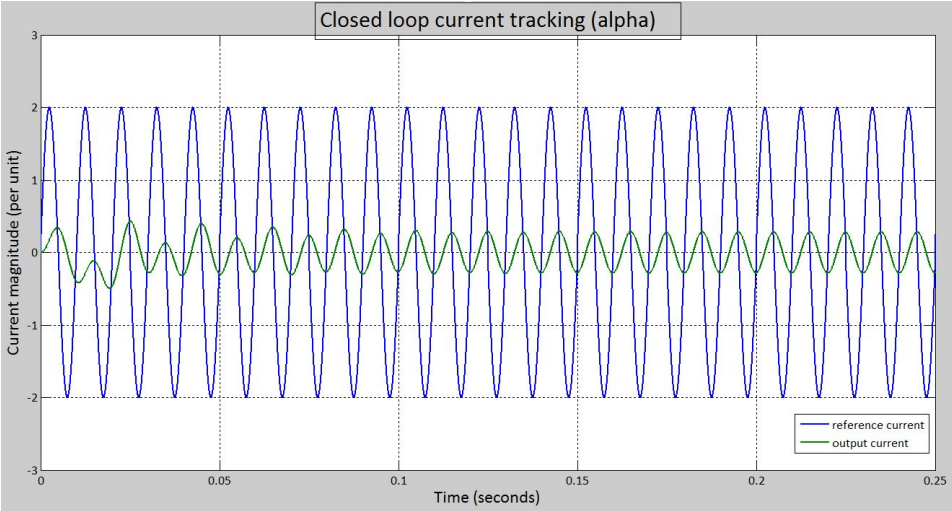


Figure 4.6: Closed loop tracking for case I for 100 Hz reference signal in alpha frame.

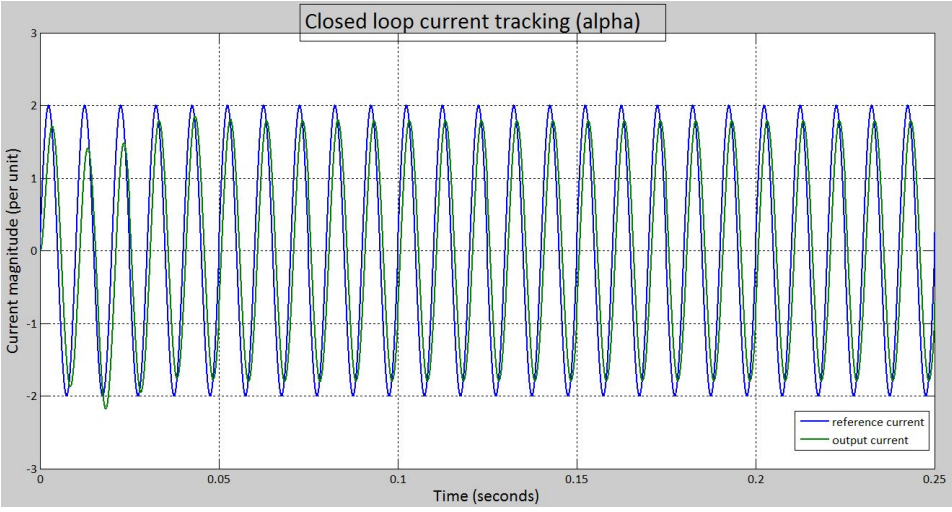


Figure 4.7: Closed loop tracking for case II for 100 Hz reference signal in alpha frame.

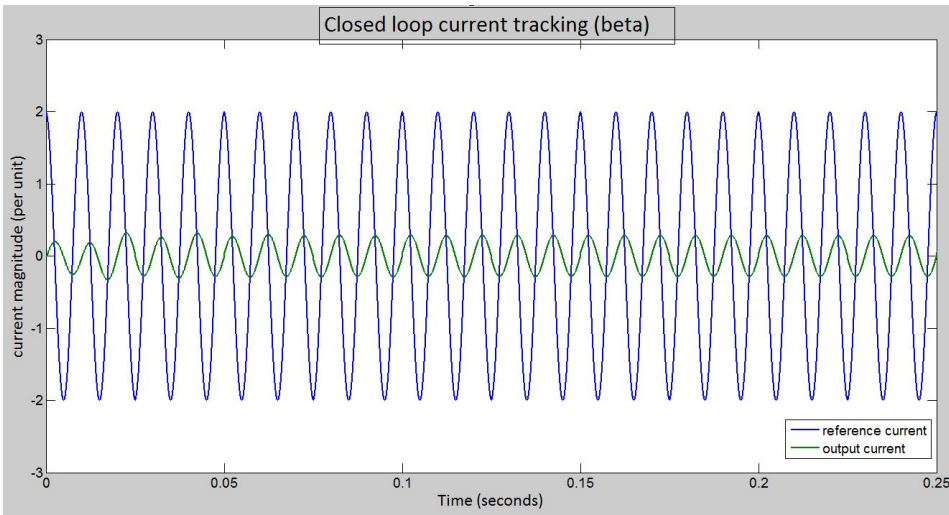


Figure 4.8: Closed loop tracking for case I for 100 Hz reference signal in beta frame.

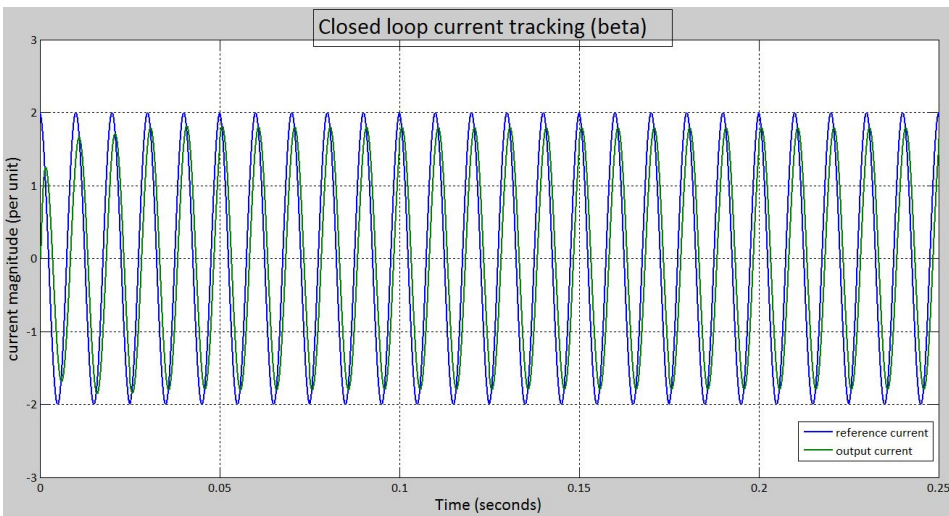


Figure 4.9: Closed loop tracking for case II for 100 Hz reference signal in beta frame.

As can be seen from the figures 4.8 and 4.9, with an increment in K_I although there was good dynamic response or faster response, the selective filtering criterion is affected.

4.2 Design of PR Voltage Controller: MATLAB Model Case Study 2

Once the inner current controller has been designed, the model is further extended to study for the outer voltage PR controller loop inclusion. The model to be studied is as shown in figure 4.10.

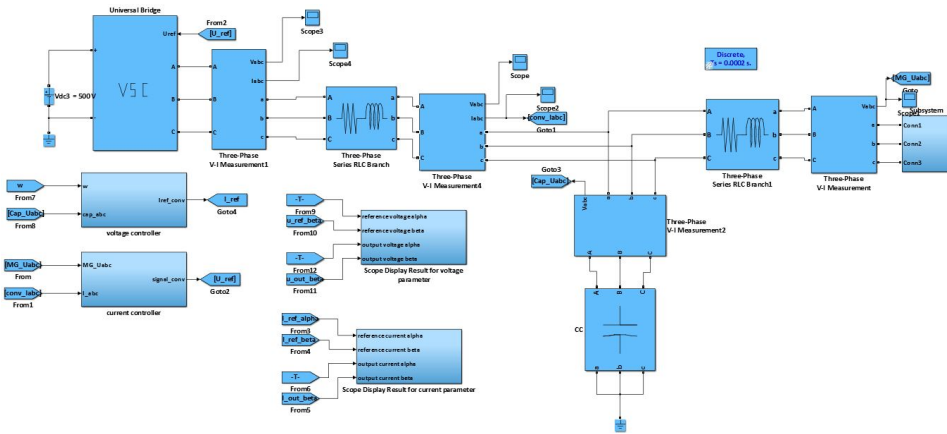


Figure 4.10: MATLAB model for testing the discretized PR voltage controller.

In figure 4.10 all parameters and connections are similar to the one for the current controller test except that it has now a capacitor block connected of value $990 \mu F$. The voltage PR controller setup is similar to that of the current controller but with different parameters as defined in the m-file attached at the appendix.

4.2.1 Model Background

The model study can be represented in terms of loop expression as shown in figure 4.11:

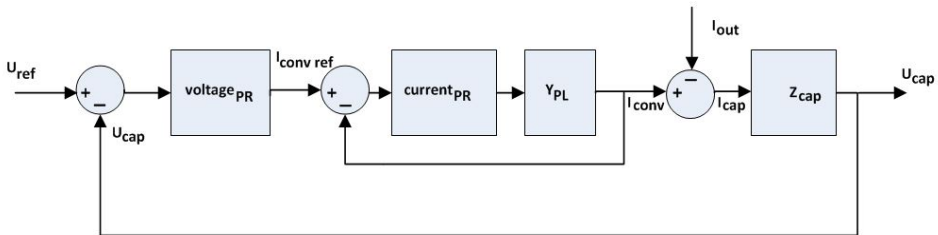


Figure 4.11: Closed loop of the voltage controller.

Y_{PL} corresponds to the admittance represented by the RL series circuit of the plant model,

Chapter 4. Controller Design

or $Y_{PL} = \frac{1}{Z_{PL}}$ where $Z_{PL} = R + sL$ is the impedance represented by the RL series circuit of the plant model.

To define the unknown parameters in these expressions, the similar approach as for current controller is followed. The closed loop result for the current controller loop replaces the current controller loop in figure 4.11. The new transfer function as seen from MATLAB is:

$$G_{currentclosedloop}(z) = \frac{0.1212z^2 - 0.2408z + 0.1197}{1.02z^4 - 3.036z^3 + 3.137z^2 - 1.241z + 0.1197} \quad (4.1)$$

The diagram can be further simplified to:

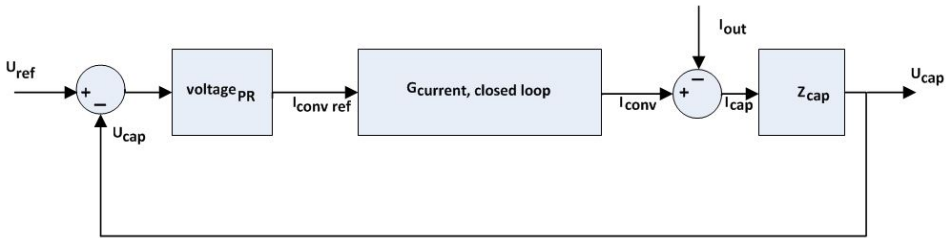


Figure 4.12: Closed loop of the voltage controller: simplified.

Now, in the figure 4.12 with a similar comparison to the current controller loop figure, the plant function can be thought to be:

$$G_{PL}(z) = G_{currentclosedloop}(z) * Z_{cap}(z) \quad (4.2)$$

ϕ'_{hv} is the delay angle to be compensated in the voltage PR controller due to the transfer function $G_{PL}(z)$.

For $K_{P_{hv}}=1$ and $K_{I_{hv}}=200$, the bode plots for nyquist and frequency stability are attached at the appendix under the section A.3, but the frequency analysis closed loop tracking and the scope results are as shown in figures 4.13 and 4.14.

4.2 Design of PR Voltage Controller: MATLAB Model Case Study 2

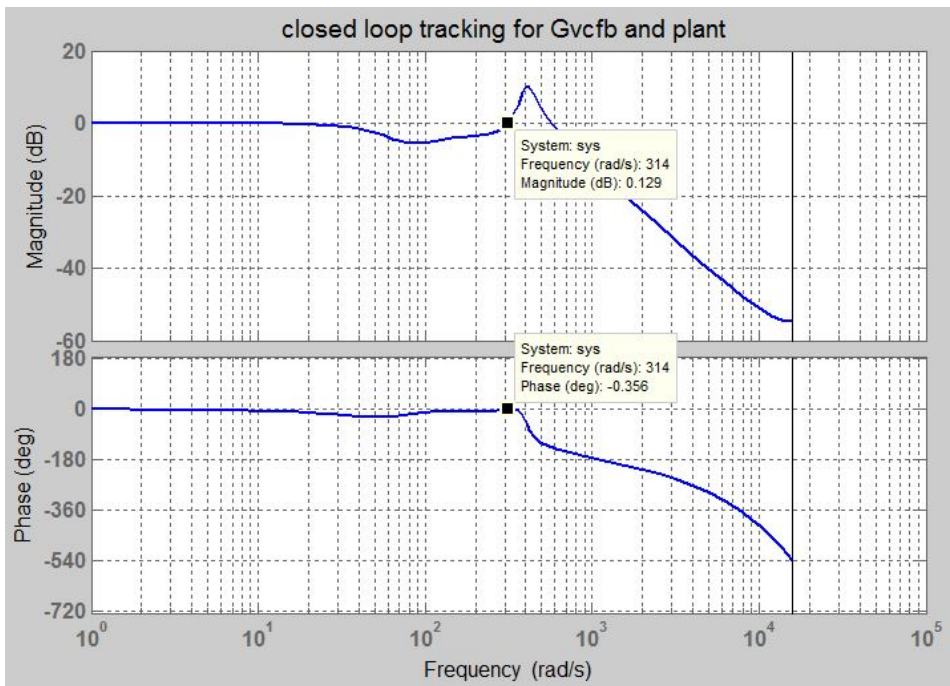


Figure 4.13: Bode plot closed loop tracking of voltage controller.

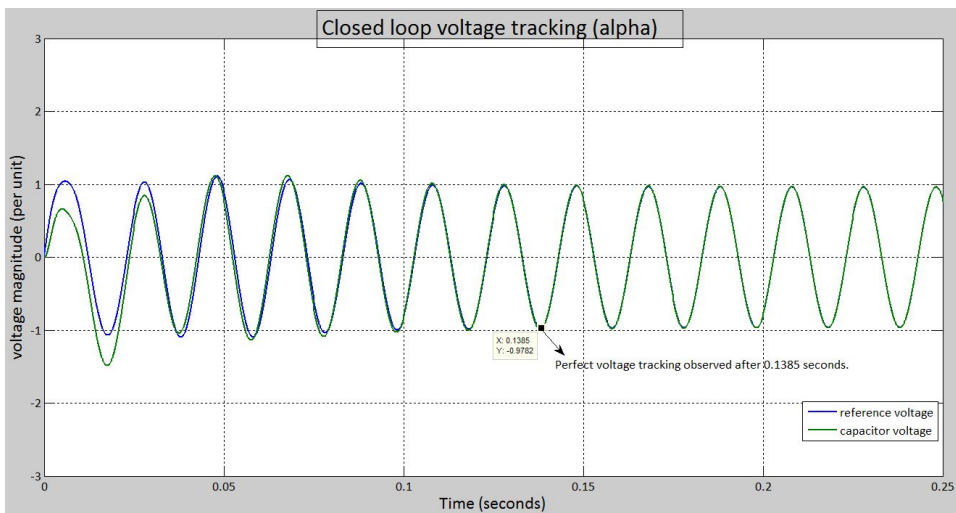


Figure 4.14: Scope result on voltage tracking.

The settling time is around 0.1385 seconds.

4.3 Design of PR Controllers: SINTEF MATLAB Model Case Study 3

First, in the extensive working MATLAB model from SINTEF, their already running PI controllers were replaced with the PR controllers designed from earlier case studies with proper settings of course. The PR current controller was first tested to see its compatibility with their working structure. The results obtained in MATLAB itself are first demonstrated here.

Later, this was extended in the testing of the voltage controller in the outer loop along with the already approved current controller. The results obtained in MATLAB are again put forward here.

Then the real lab setup implementation begins with the interfacing OPAL-RT in action. The laboratory setup is discussed in chapter 5.

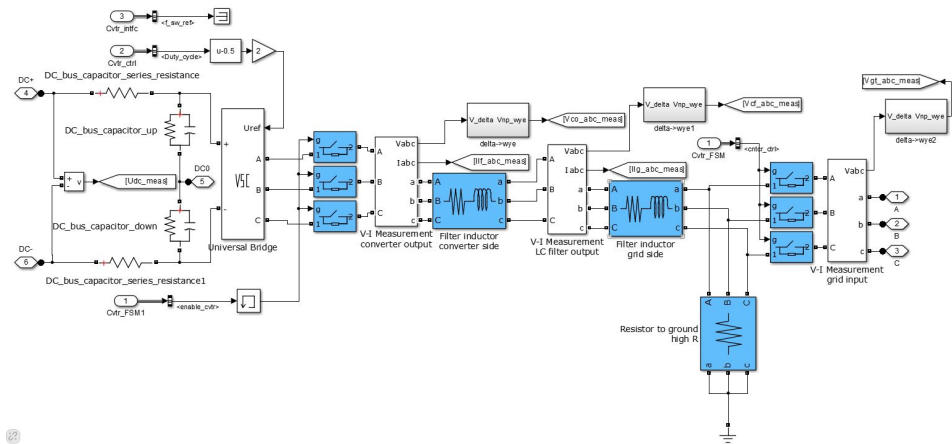


Figure 4.15: Electrical setup in SINTEF MATLAB model for the current controller.

Figure 4.15 is a part of the overall SINTEF MATLAB model which shows the electrical setup on which the current controller is designed.

4.3.1 Results for the Current Controller only

The results after the testing of a current controller in the SINTEF model are put forward here. The details of the MATLAB model are not mentioned but the electrical setup in the MATLAB model is as shown in figure 4.15. In figure 4.15, electrical setup for current controller testing is modelled. It has a converter connected to the filter inductors and then a resistor that is grounded. A three phase contactor is present between the converter and filter inductor while another set is present between the second filter inductor and the load which is not shown here in figure 4.15.

4.3 Design of PR Controllers: SINTEF MATLAB Model Case Study 3

The base, parameter and rated values for this model are as indicated in the tables 3.3, 3.4 and 3.5 respectively.

The figures in 4.16 and 4.17 show the tracking of the reference current by the output current with the implementation of the current controller while the figures are zoomed in to see the nature of the graphs in details as mentioned in the figures in 4.18 and 4.19.

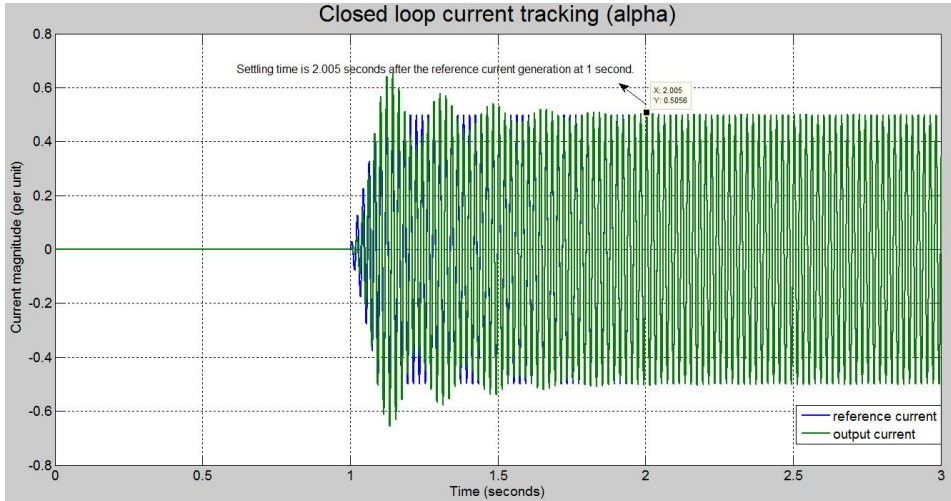


Figure 4.16: Closed loop current tracking for 50 Hz reference signal in alpha frame .

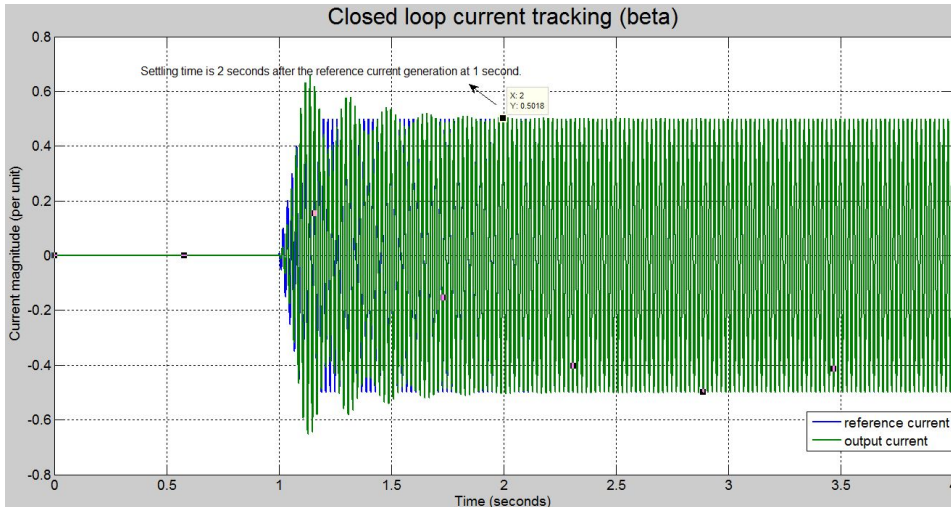


Figure 4.17: Closed loop current tracking for 50 Hz reference signal in beta frame .

It is seen that it takes around 2 seconds for the settling period and that there are some

Chapter 4. Controller Design

peaks at the start. With a different set of proportional and resonant gains, better result can be obtained as the result obtained for a proportional and resonant gains of 1 and 1200 respectively verifies as shown in figure 4.20. The settling time is around 1.24 seconds.

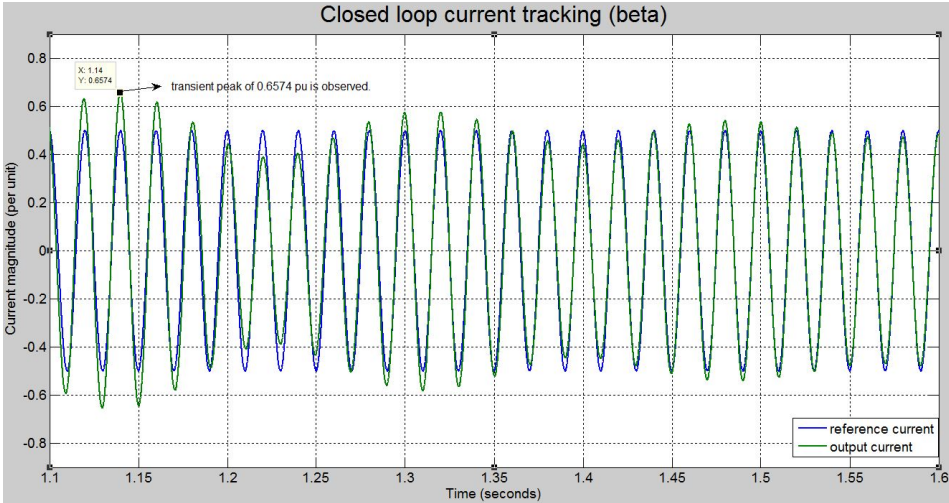


Figure 4.18: Zoomed in look at the transient peak observation in beta frame.

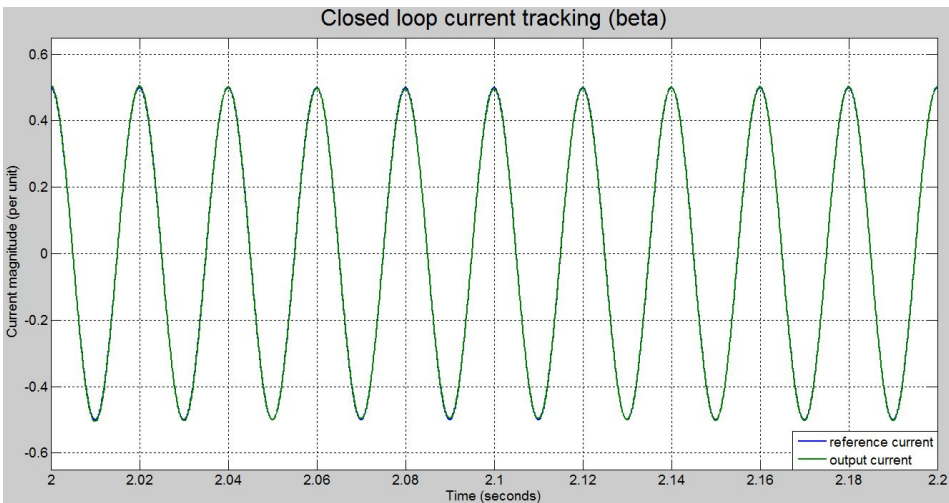


Figure 4.19: Zoomed in look at the steady state observation in beta frame.

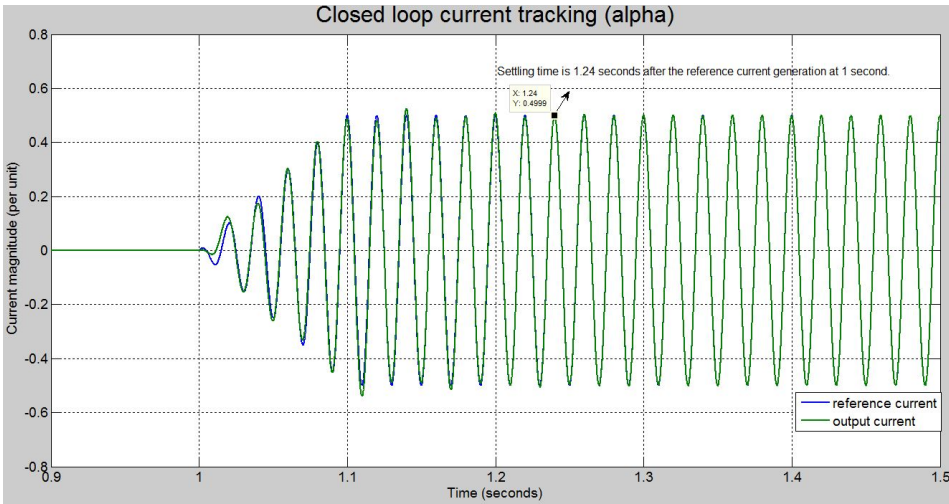


Figure 4.20: Working of the current controller for proportional and resonant gains of 1 and 1200 respectively in alpha frame.

4.3.2 Results for the Voltage Controller Cascaded with Current Controller

After the successful testing of the current controller, the testing was extended for a cascaded outer voltage controller with the already approved current controller. The electrical setup in the MATLAB model is as shown in the figure 4.21. It is similar to the model in figure 4.15 but with the addition of a capacitor parallelly between the two filter inductors.

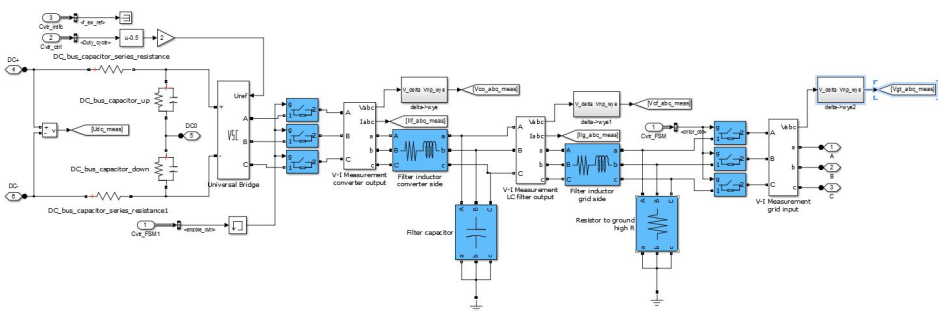


Figure 4.21: Electrical setup in SINTEF MATLAB model for the voltage controller.

For the given parameters of the current and voltage controllers: current proportional gain, $k_p=1$ and current resonant gain, $k_i=500$ and voltage proportional gain, $k_p=1$ and voltage resonant gain, $k_i=25$ the results were likewise put forward in the figures 4.22 and 4.23:

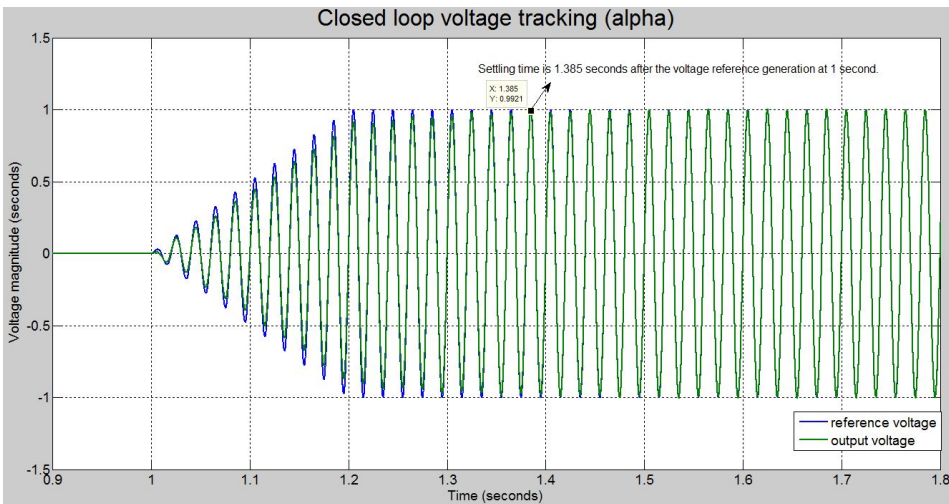


Figure 4.22: Working of the voltage controller.

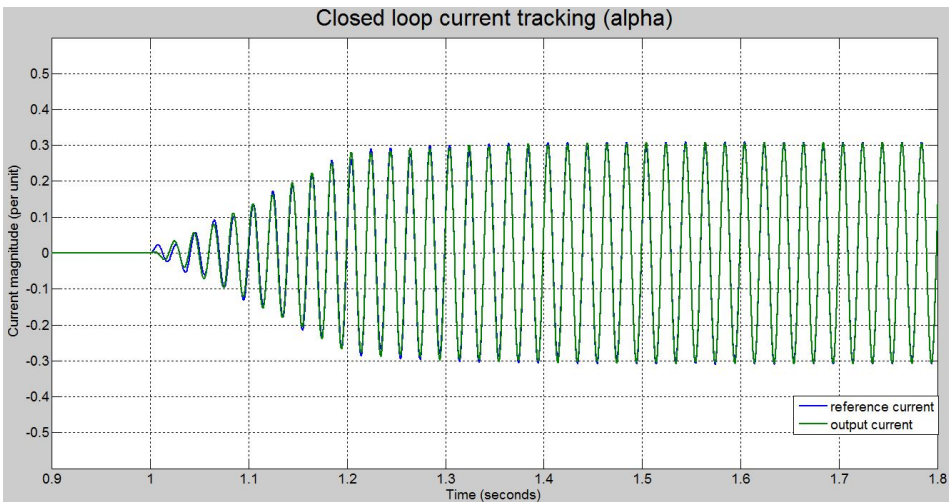


Figure 4.23: Working of the current controller cascaded with a voltage controller.

4.3.3 Testing with Prototype Parameters

In order to compare results obtained from simulation and the actual laboratory experiments, the same parameters as applicable to the laboratory setup are introduced in the SINTEF MATLAB model. This means filter parameters of 2 mH and $50\text{ }\mu\text{F}$ for a three phase balanced resistive load of $63\text{ }\Omega$.

The results of voltage tracking and current tracking are shown in figures 4.24 and 4.25

respectively.

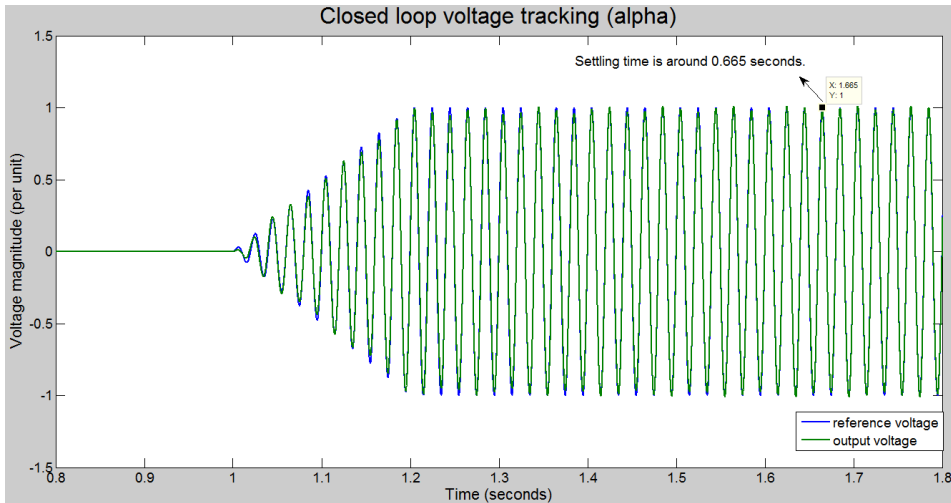


Figure 4.24: Closed loop voltage tracking in alpha frame.

Figure 4.24 shows that the settling time after a transient phase for a PR voltage controller output is 0.665 s . The tracking of current controller output is a bit noisier than that for the voltage controller as seen in 4.25 but it does settle down later on the steady state as shown in figure 4.26.

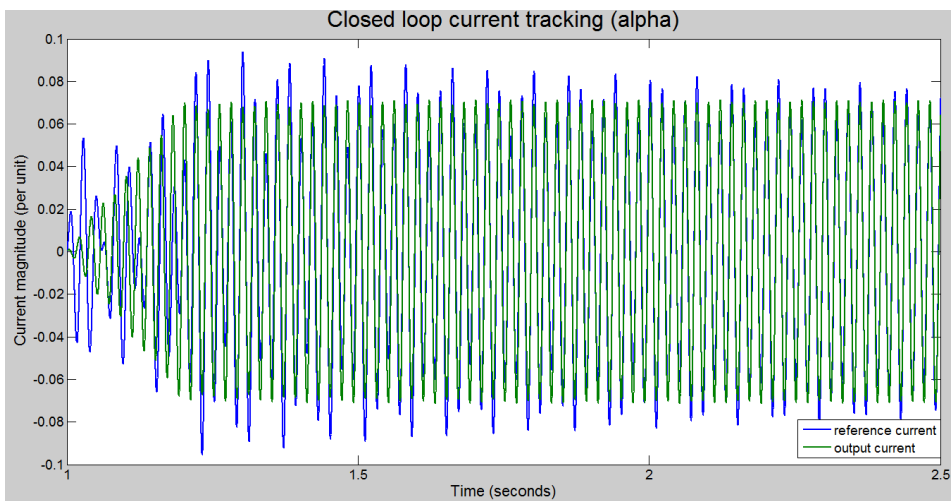


Figure 4.25: Closed loop current tracking in alpha frame.

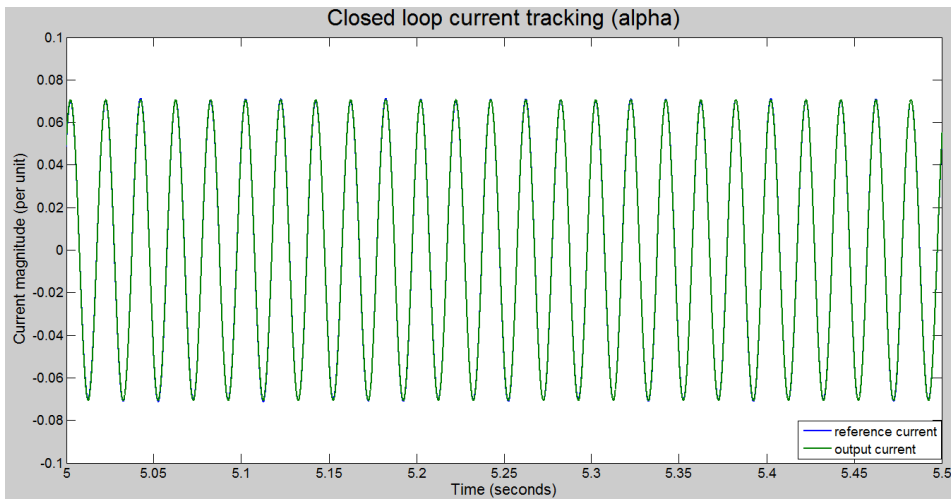


Figure 4.26: Zoomed in view at the closed loop current tracking in alpha frame in steady state.

With this third case study controller design, pre-laboratory tasks were also completed and the final phase of actual laboratory implementation was carried out which is further explained in detail in the next chapter to follow.

Laboratory Work

5.1 General Layout

The laboratory implementation part is covered in this chapter. This is the second or the final phase where the designed discrete PR controllers are tested in actual laboratory setup. The schematic diagram of the laboratory setup is as shown in the figure 5.1.

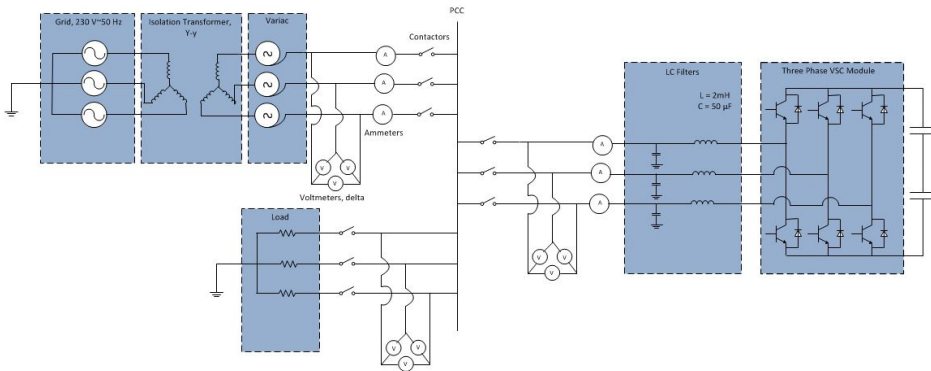


Figure 5.1: Schematic representation of the laboratory setup.

In the figure 5.1, a resistive load is being fed at PCC from both grid and a three phase VSC module. There are three sets of three phase contactors for each of the three elements: grid side, converter side and the load side. A LC filter is present on the converter side with an inductance of 2 mH and a capacitance of $50\text{ }\mu\text{F}$. An isolation transformer at the grid side in star-star connection relates the grid side of 230 V , 50 Hz through a variac control to the PCC. Three sets of delta connected three phase voltmeters are placed as shown in the figure 5.1 for measurement purpose while two sets of three phase ammeters are placed to measure grid side current to PCC and converter side current to PCC. The laboratory implementation

is in an islanded operation mode, that is, there is no grid connection. This is the general layout of the laboratory setup.

5.1.1 Components used in the Laboratory Setup

The components used in the laboratory setup are shown in the appendix under section A.4. Here is a list of the name of those equipments.

- Sintef Energy Voltage sensor box, SINTEF Energi AS 105 – 0034.
- DC Voltage measurement, SINTEF C02 – 0376.
- Current measurement, *LEM LA205 – S17108* (Swiss made).
- Three phase filter inductors, 2 *mH*, SIEMENS, Type: *T266.35.156/4646.2*, No. *L6 – 080302*.
- Three phase star connected filter capacitors, 50 μF .
- Three phase resistive load, 63 Ω .

5.2 Results

5.2.1 Test Outcomes of a Current Controller

First the current controller was tested for a current proportional gain, $k_p=1$ and current resonant gain, $k_i=300$. The results viewed from oscilloscope for this test are shown in figures 5.2, 5.3 and 5.4.

Figure 5.2 shows the transient response of the output current to the change in the reference current. As seen in the figure, the settling time is quite large which can be further improved with another set of proportional and resonant gains.

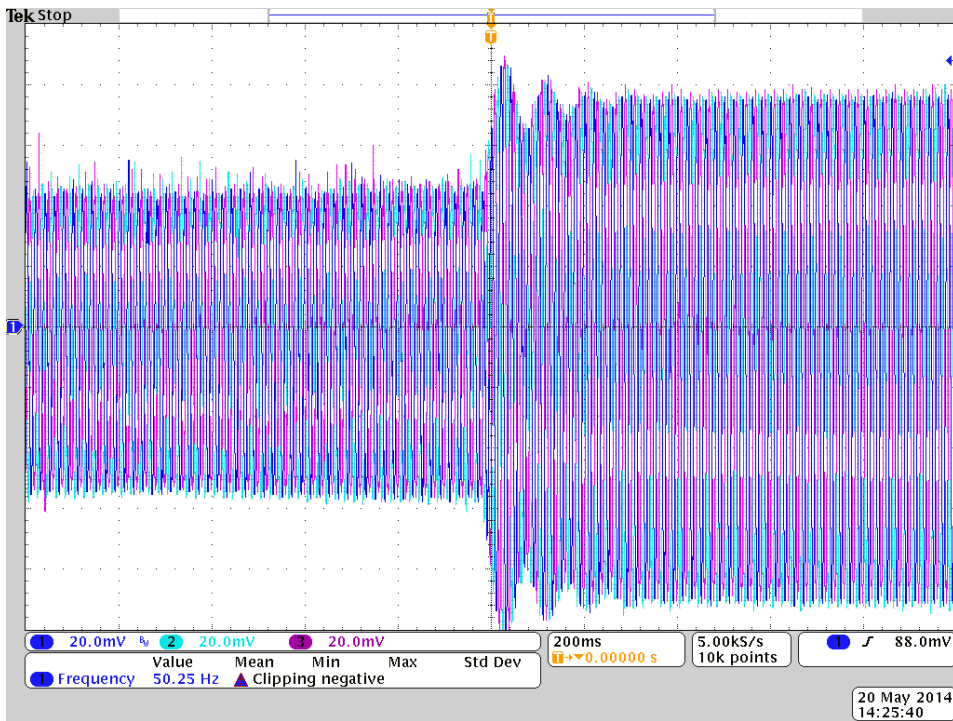


Figure 5.2: Transient response to the change in reference current.

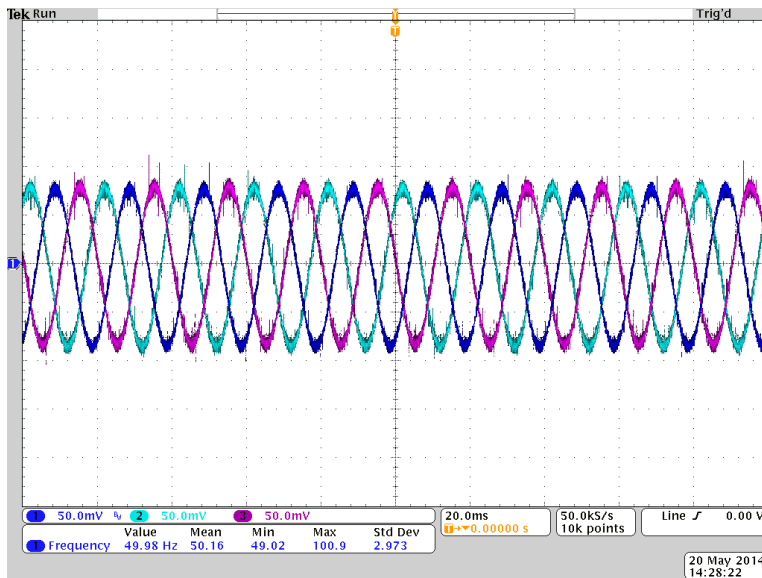


Figure 5.3: Closer look at the three phase current waveforms.

Chapter 5. Laboratory Work

Figure 5.3 gives a zoomed in look to the three phase current waveforms while figure 5.4 shows the switching action of the three phase VSC module to generate these current waveforms.

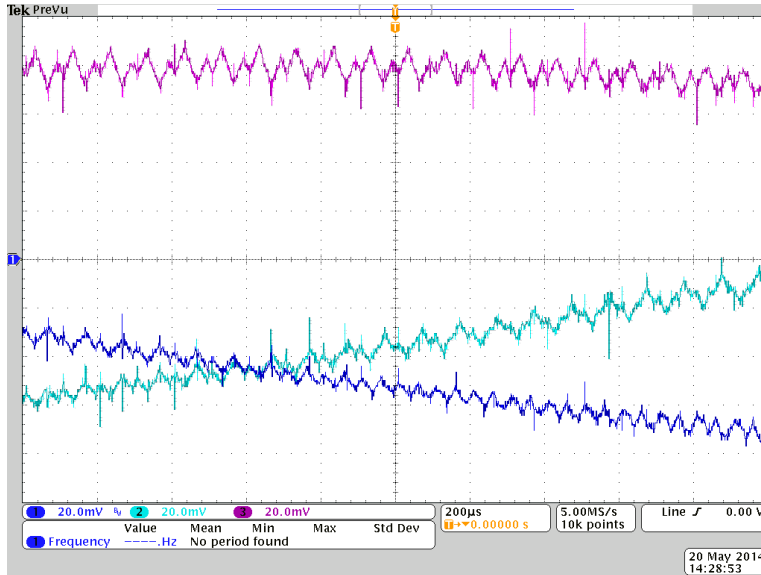


Figure 5.4: Switching in each of the three phases of current.

5.2.2 Test Outcomes of a Cascaded Voltage Controller with a Current Controller

The voltage controller with a voltage proportional gain, $k_p=1$ and voltage resonant gain, $k_i=10$ was tested with the current controller of previous sets of gain values. The results viewed from oscilloscope for this test are shown in figures 5.5 and 5.6.

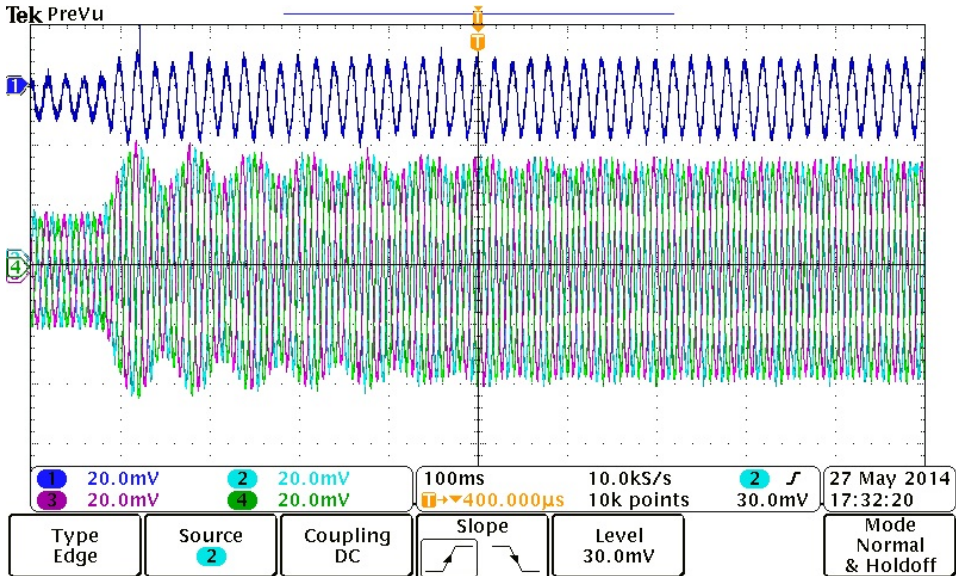


Figure 5.5: Transient response to the change in reference voltage.

Figure 5.5 shows the transient response to a change in the reference voltage. The single dark blue waveform on the top of the scope is one of the current waveforms while the lower waveforms are the three phase voltage waveforms. The settling time is poor at around 0.9 s but this can be improved with another choice of gains sets. Figure 5.6 gives a closer look into the three phase waveforms of the voltage and one of the three phase waveforms of the current.

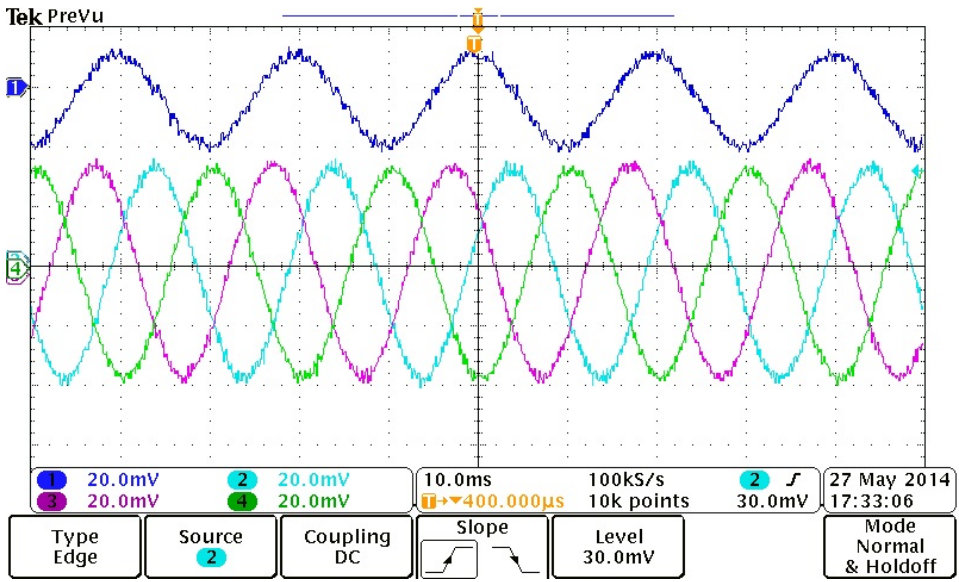


Figure 5.6: Closer look at the three phase voltage waveforms.

Discussion

A successful implementation of discretized PR controllers was carried out. It began from the study of PR controllers in a continuous domain which was later extended to discrete domain with three phases of work levels for digital implementation. The s-domain study was almost 90 % done in the specialization course project in Autumn 2013 and some of its remaining result, specially the parallel operation model of two units with P-f and Q-U droops, were included in this final thesis.

For continuous domain, it was basically Josep M. Guerrero's papers that were being followed and studied while for the discretization part, Alejandro G. Yepes' papers were referred to.

Discretization

Discretization is a tricky job more so when it comes to the discretization of resonant controllers such as PR controllers because they have high selectivity such that their performance is very much dependent on the accuracy of the resonant frequency. Hence, PR controllers are specially sensitive to the discretization process courtesy their narrow band and infinite gain features at the resonant frequency [20].

For the digital implementation of the PR controllers, two integrator method has been implemented so as to achieve frequency adaptation with less computational load but then this implementation suffered from distinct errors both in the resonant frequency and in the phase lead provided by delay compensation resulting in doubts over perfect tracking and stability issues [20]. Hence, delay compensation technique was employed to improve this situation.

Discretized PR controllers were tested and analyzed through three levels, firstly in a self-made MATLAB model (section 4.1 and section 4.2) and then in the SINTEF MATLAB model (section 4.3), and finally implementation in the laboratory. The results from all the

three steps of analysis have been put and discussed in details in the previous chapters.

Discussion of case study 1

From case study 1 in section 4.1, it was observed that the rate of magnitude tracking depended on the value of the resonant gain parameter, K_I . The larger the value of K_I , the faster was the magnitude tracking as depicted in figures 4.2 and 4.3. But then, it should be kept in mind that K_I should be tuned to obtain an adequate compromise between selective filtering and dynamic response as showcased in figures 4.6 and 4.7. Hence, from case study 1 in section 4.1, for a discretized PR current controller, the roles of resonant gain parameter K_I on the output result was analyzed.

Discussion of case study 2

The case study 2 in section 4.2 followed the design of PR voltage controller cascaded with a PR current controller. Based on the same design concept as the PR current controller, PR voltage controller was designed and its frequency analysis on closed loop tracking in figure 4.13 was confirmed by the scope result obtained after simulation as shown in figure 4.14.

Discussion of case study 3

The study model as well as the electrical parameters were different for the three case studies but case study 3 in section 4.3 was designed for the laboratory model. In the third case study, when current controller was tested alone, as confirmed by the results of case study 1, larger value of the resonant gain parameter, K_I accounted for faster tracking response as compared from figures 4.16 and 4.20. Also, for the voltage controller when cascaded with the current controller, the results obtained were satisfactory as seen in the reference tracking by both the voltage and current output of the system in figures 4.22 and 4.23 respectively.

Discussion of the laboratory setup

The experiments in the laboratory verified the implementation of PR controllers. Although the transient behaviour was a bit questionable, it did verify the operation of PR controllers. The transient behaviour can be improved on with further studies and proper selection of the gain parameters. The results obtained from the laboratory implementation quite agreed on the results from the third case study.

Comparison between simulation and experiment results

For the same parametric condition, the result obtained from MATLAB simulation in 4.24 and the result obtained from laboratory experiment in 5.5 showed similar nature, that is, near-perfect tracking of voltage at steady state and an appreciable settling time during the

transient state. The settling time was seen to be 0.665 s from the simulation result while it was 0.9 s from the laboratory result. This difference could be possible because of the non-ideal electrical components as inductors used in laboratory setup or some instrumental error.

Feasibility of PR controllers

The results obtained from the laboratory setup can be improved in the part of settling time, but as of now, the main target was to implement successfully discretized PR controllers, which has been done in this thesis for an islanded operation mode. Improving the settling time can be one of the tasks to be performed in later time but other than that, the discretization approach for PR controllers has given good enough results for their digital implementation.

Chapter 6. Discussion

Conclusion

Although there had been a conclusion of the PR controllers in continuous domain in previous report, that conclusion cannot be directly applied to the digital implementations but the discretization method approached for the PR controllers with two integrators method gives a definite conclusion that PR controllers are applicable in digitalized environment and their implementation in grid system improves or adds up in the smart grid functionality as mentioned in chapter 1.

From case studies 1 and 2 under section 4.1 and section 4.2 respectively, the PR controllers designed were :

$$G_{cfb}(z) = \frac{z^2 - 1.987z + 0.9873}{z^2 - 1.996z + 1} \quad (7.1)$$

$$G_{vcfb}(z) = \frac{z^2 - 1.956z + 0.9605}{z^2 - 1.996z + 1} \quad (7.2)$$

Chapter 7. Conclusion

Future Work

With the above discussion and conclusion on the work done so far in this thesis, Spring 2014, there still remains work to be done. These future tasks can be bulleted in the list below:

- Synchronization to the main grid in continuous domain and discrete domain both.
- Testing of non-linear and unbalanced loads.
- Improvement in the settling time.

Chapter 8. Future Work

Bibliography

- [1] O. of Electricity Delivery and E. R. S. G. R. Program, “Summary report: 2012 doe microgrid workshop,” (Chicago, Illinois), July 30-31 2012.
- [2] R. Lasseter, “Smart distribution: Coupled microgrids,” *Proceedings of the IEEE*, vol. 99, no. 6, pp. 1074–1082, 2011.
- [3] I. R. Hatziaargyriou Nikos, Asano Hiroshi and M. Chris, “Microgrids,” 2007.
- [4] J. Guerrero, J. Vasquez, J. Matas, L. de Vicua, and M. Castilla, “Hierarchical control of droop-controlled ac and dc microgrids -a general approach toward standardization,” *Industrial Electronics, IEEE Transactions on*, vol. 58, no. 1, pp. 158–172, 2011.
- [5] T. Logenthiran and D. Srinivasan, “Intelligent management of distributed storage elements in a smart grid,” in *Power Electronics and Drive Systems (PEDS), 2011 IEEE Ninth International Conference on*, pp. 855–860, 2011.
- [6] J. Peas Lopes, C. Moreira, and A. Madureira, “Defining control strategies for microgrids islanded operation,” *Power Systems, IEEE Transactions on*, vol. 21, no. 2, pp. 916–924, 2006.
- [7] M. Surprenant, I. Hiskens, and G. Venkataramanan, “Phase locked loop control of inverters in a microgrid,” in *Energy Conversion Congress and Exposition (ECCE), 2011 IEEE*, pp. 667–672, 2011.
- [8] D. F. Simpson-Porco John W. and B. Francesco, “Droop-controlled inverters in microgrids are kuramoto oscillators,” 2012.
- [9] R. Teodorescu, F. Blaabjerg, M. Liserre, and P. Loh, “Proportional-resonant controllers and filters for grid-connected voltage-source converters,” *Electric Power Applications, IEE Proceedings*, vol. 153, no. 5, pp. 750–762, 2006.
- [10] M. Castilla, J. Miret, J. Matas, L. Garcia de Vicuna, and J. Guerrero, “Control design guidelines for single-phase grid-connected photovoltaic inverters with damped resonant harmonic compensators,” *Industrial Electronics, IEEE Transactions on*, vol. 56, no. 11, pp. 4492–4501, 2009.

-
- [11] J. Guerrero, J. Matas, L. de Vicua, M. Castilla, and J. Miret, "Wireless-control strategy for parallel operation of distributed-generation inverters," *Industrial Electronics, IEEE Transactions on*, vol. 53, no. 5, pp. 1461–1470, 2006.
- [12] J. Guerrero, L. Garcia de Vicuna, J. Matas, M. Castilla, and J. Miret, "Output impedance design of parallel-connected ups inverters with wireless load-sharing control," *Industrial Electronics, IEEE Transactions on*, vol. 52, no. 4, pp. 1126–1135, 2005.
- [13] T. Vandoorn, B. Renders, B. Meersman, L. Degroote, and L. Vandevelde, "Reactive power sharing in an islanded microgrid," in *Universities Power Engineering Conference (UPEC), 2010 45th International*, pp. 1–6, 2010.
- [14] J. Guerrero, J. Matas, L. G. de Vicuna, M. Castilla, and J. Miret, "Decentralized control for parallel operation of distributed generation inverters using resistive output impedance," *Industrial Electronics, IEEE Transactions on*, vol. 54, no. 2, pp. 994–1004, 2007.
- [15] W. Yao, M. Chen, J. Matas, J. Guerrero, and Z. ming Qian, "Design and analysis of the droop control method for parallel inverters considering the impact of the complex impedance on the power sharing," *Industrial Electronics, IEEE Transactions on*, vol. 58, no. 2, pp. 576–588, 2011.
- [16] A. Yepes, F. Freijedo, J. Doval-Gandoy, O. Lopez, J. Malvar, and P. Fernandez-Comesaa, "Effects of discretization methods on the performance of resonant controllers," *Power Electronics, IEEE Transactions on*, vol. 25, pp. 1692–1712, July 2010.
- [17] A. Yepes, F. Freijedo, O. Lopez, and J. Doval-Gandoy, "High-performance digital resonant controllers implemented with two integrators," *Power Electronics, IEEE Transactions on*, vol. 26, pp. 563–576, Feb 2011.
- [18] A. Vidal, F. Freijedo, A. Yepes, P. Fernandez-Comesana, J. Malvar, O. Lopez, and J. Doval-Gandoy, "Assessment and optimization of the transient response of proportional-resonant current controllers for distributed power generation systems," *Industrial Electronics, IEEE Transactions on*, vol. 60, pp. 1367–1383, April 2013.
- [19] A. Yepes, F. Freijedo, J. Doval-Gandoy, O. Lopez, J. Malvar, and P. Fernandez-Comesana, "On the discrete-time implementation of resonant controllers for active power filters," in *Industrial Electronics, 2009. IECON '09. 35th Annual Conference of IEEE*, pp. 3686–3691, Nov 2009.
- [20] A. G. Yepes, "Digital resonant current controllers for voltage source converters," 2011.
- [21] A. Yepes, F. Freijedo, P. Fernandez-Comesana, J. Malvar, O. Lopez, and J. Doval-Gandoy, "Performance enhancement for digital implementations of resonant controllers," in *Energy Conversion Congress and Exposition (ECCE), 2010 IEEE*, pp. 2535–2542, Sept 2010.
- [22] O. R. T. website, "Academic and research power systems and power electronics real time simulation," 2014.

-
- [23] M. Savaghebi, J. Vasquez, A. Jalilian, J. Guerrero, and T.-L. Lee, "Selective harmonic virtual impedance for voltage source inverters with lcl filter in microgrids," in *Energy Conversion Congress and Exposition (ECCE), 2012 IEEE*, pp. 1960–1965, 2012.

Appendix A

Simulink models

A.1 MATLAB Simulink Model for Parallel Two Units Standalone System

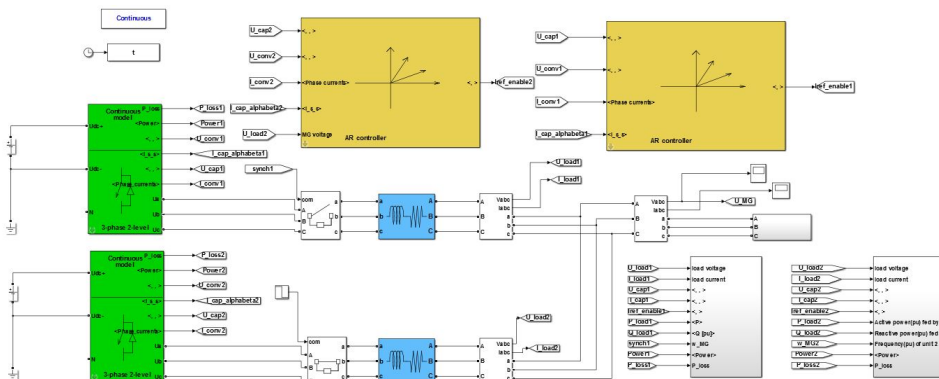


Figure A.1: Simulink model of two parallel units system.

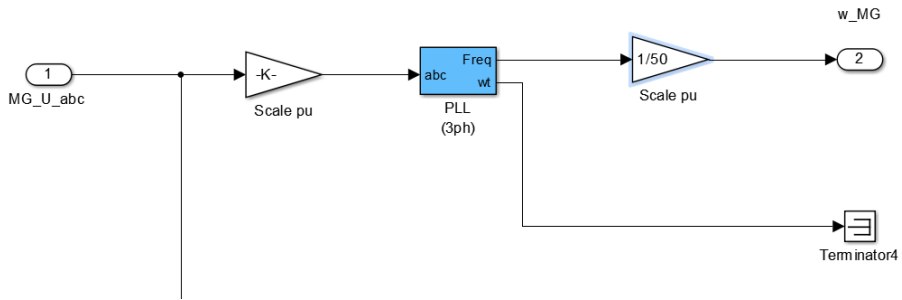


Figure A.2: PLL with PID implementation from MATLAB library.

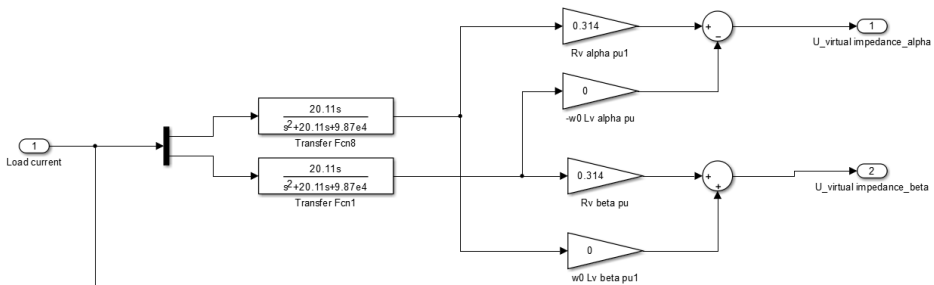


Figure A.3: Virtual impedance implementation in alpha-beta frame for resistive output impedance.[23]

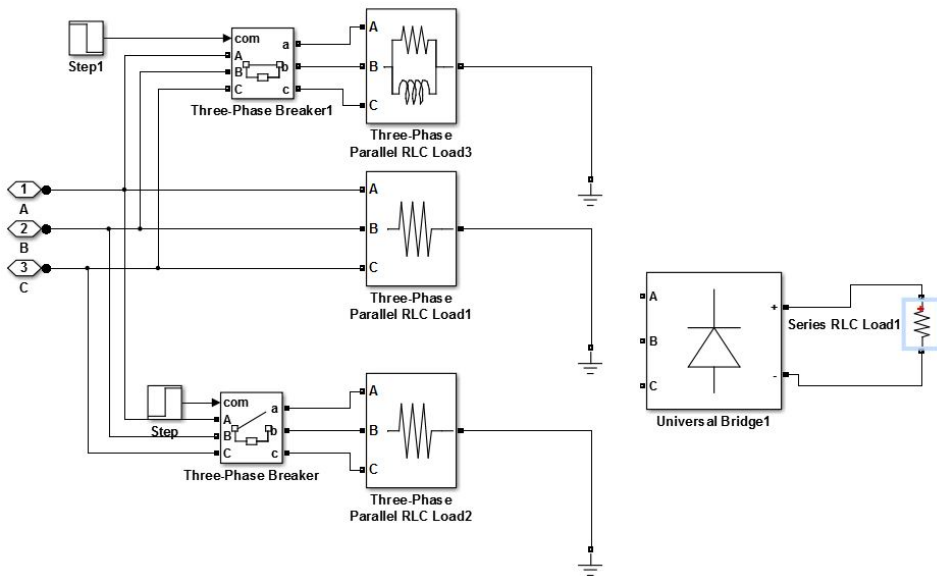


Figure A.4: Different types of load tested.

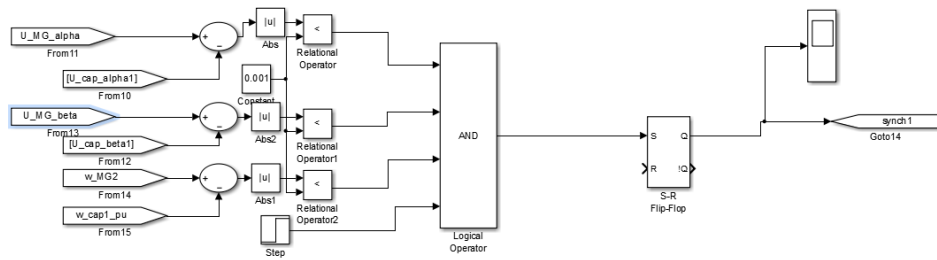


Figure A.5: Synchronization control block.

The PR controller:

$$h_0 = \frac{44.42s}{s^2 + 44.42s + 9.87e4} \quad (\text{A.1})$$

provides the fundamental component selection.

A.1.1 Three Phase Current Supplied to the Load by the Two Parallel Units

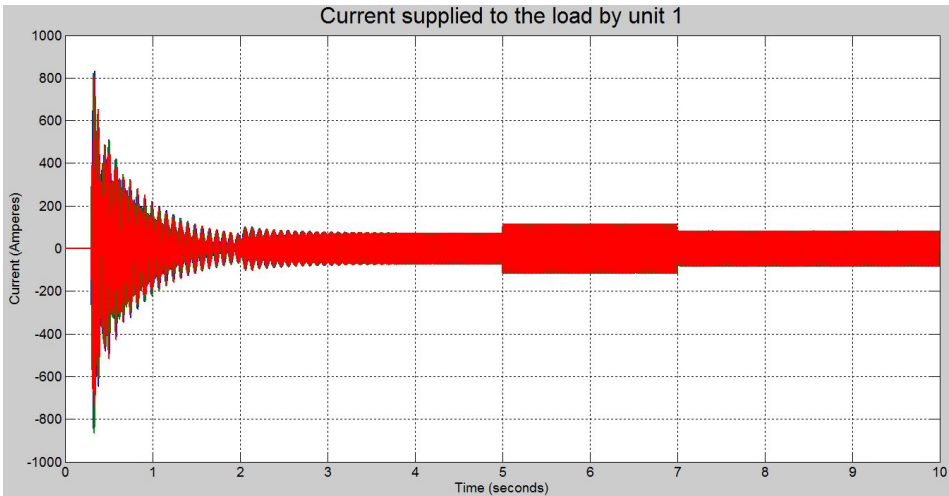


Figure A.6: Current in Amps supplied by unit 1 for a switched load demand.

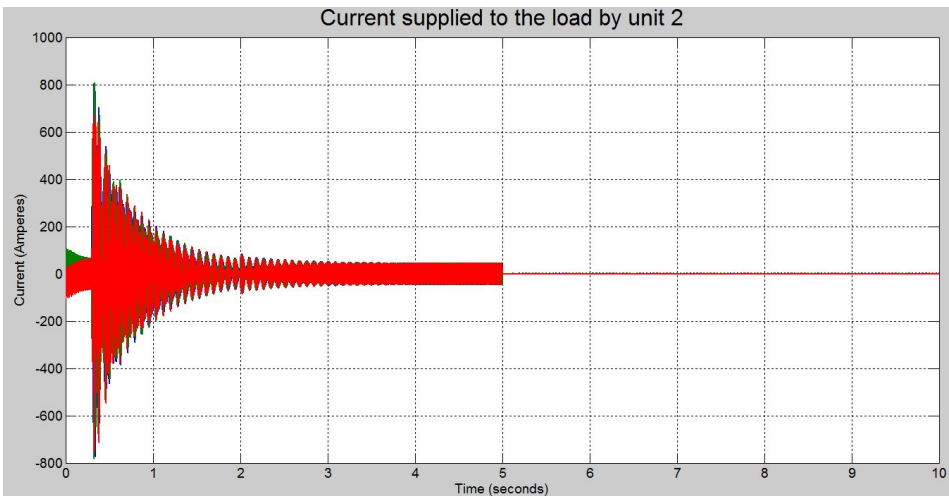


Figure A.7: Current in Amps supplied by unit 2 for a switched load demand.

A.1.2 Clarke Transformation

For a balanced condition the Clarke transformation is:

$$i_{\alpha}(t) = i_a(t) \tag{A.2}$$

$$i_{\beta}(t) = \frac{i_b(t)}{\sqrt{3}} - \frac{i_c(t)}{\sqrt{3}} \quad (\text{A.3})$$

A.2 Detailed Connctions of the Masked Blocks for Figure 4.1 in Chapter 4

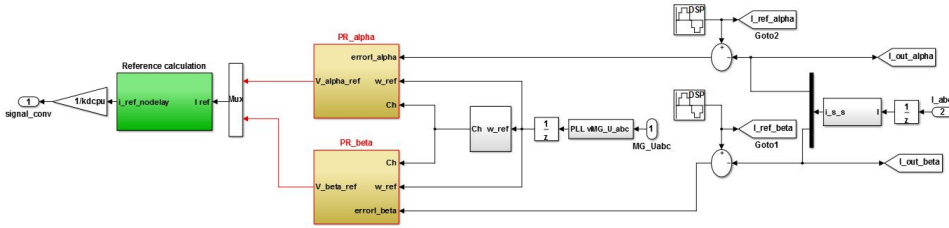


Figure A.8: Details inside current controller block in figure 4.1.

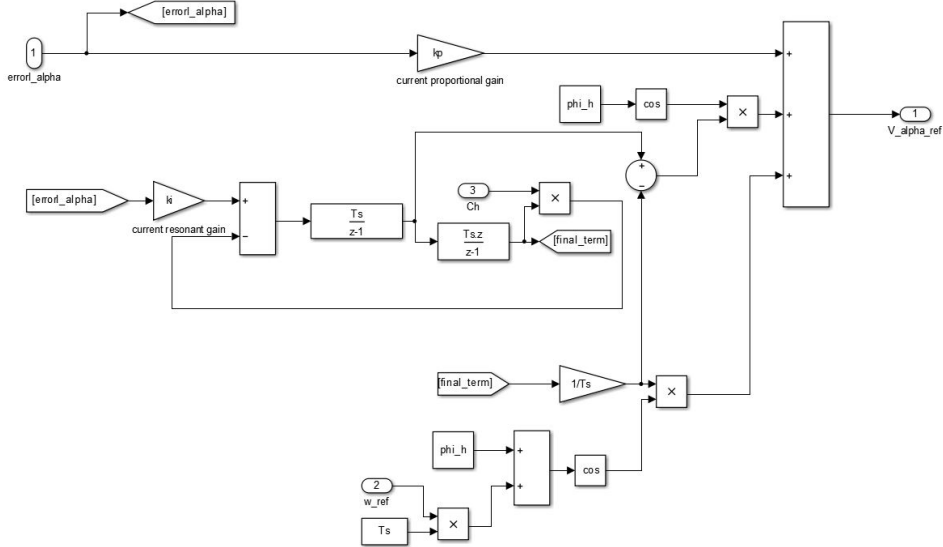


Figure A.9: Details inside PR alpha block in figure A.8.

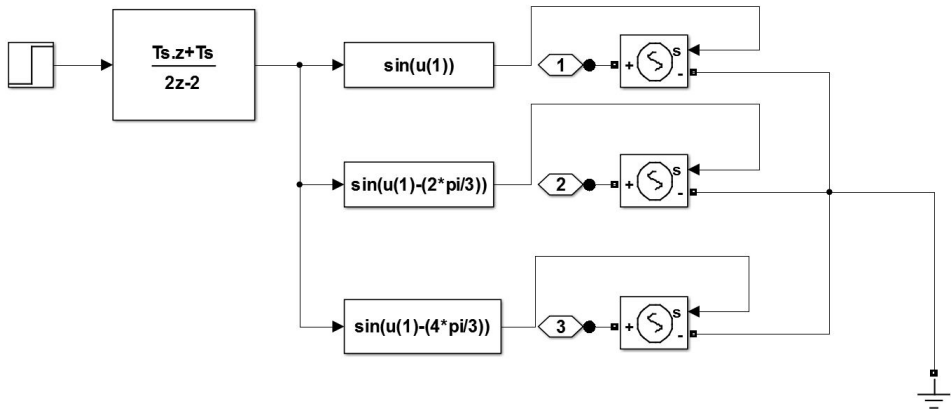


Figure A.10: Details inside subsystem block in figure 4.1.

A.3 Stability and Tracking Analysis Results for Chapter 4

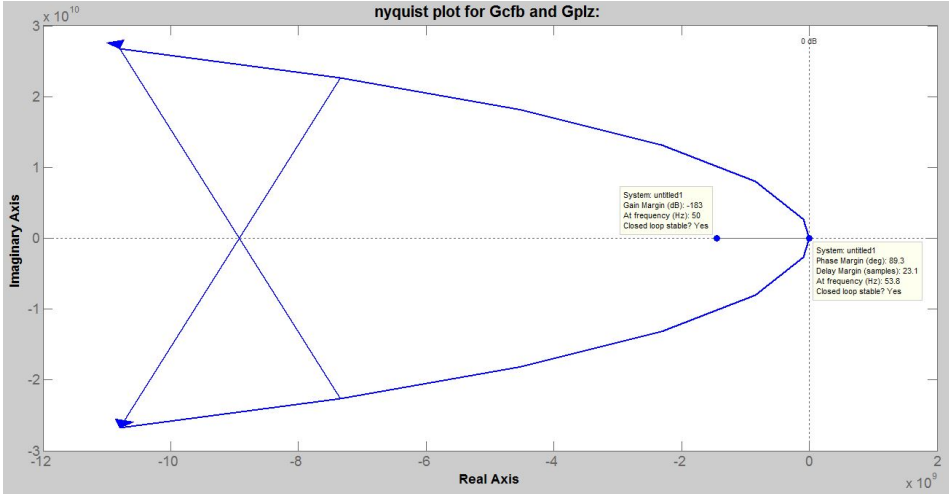


Figure A.11: Nyquist stability plot for case I.

Figures A.11 and A.12 show the stable feature of the current controller via nyquist criterion and frequency stability analysis respectively for the gain parameter set of $K_P=0.08$ and $K_I=25$ while for the same gain parameter set figure A.13 shows the tracking nature of the current controller via the frequency plot analysis.

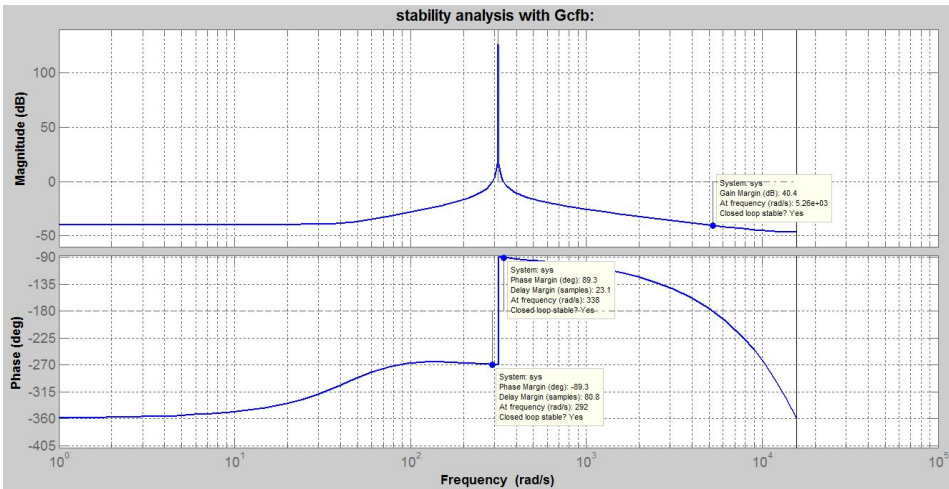


Figure A.12: Frequency stability plot analysis for case I.

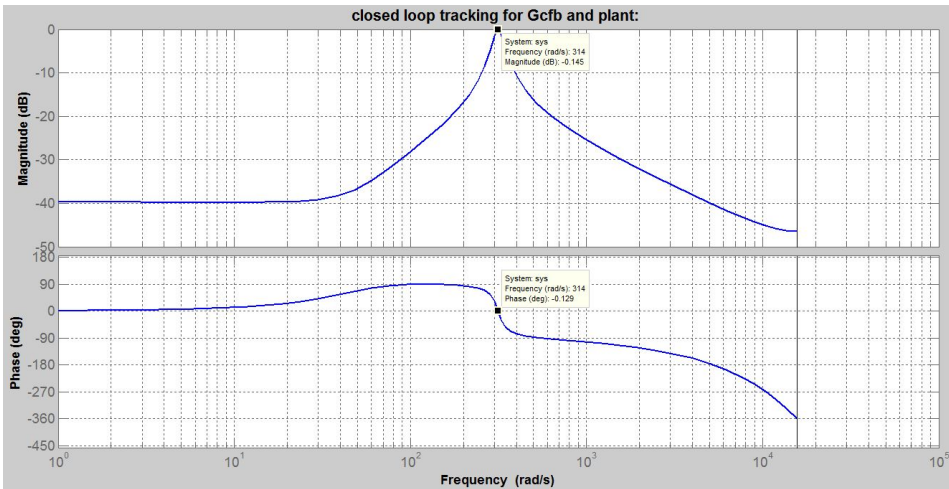


Figure A.13: Tracking nature of the transfer function of the discretized PR current controller for case I.

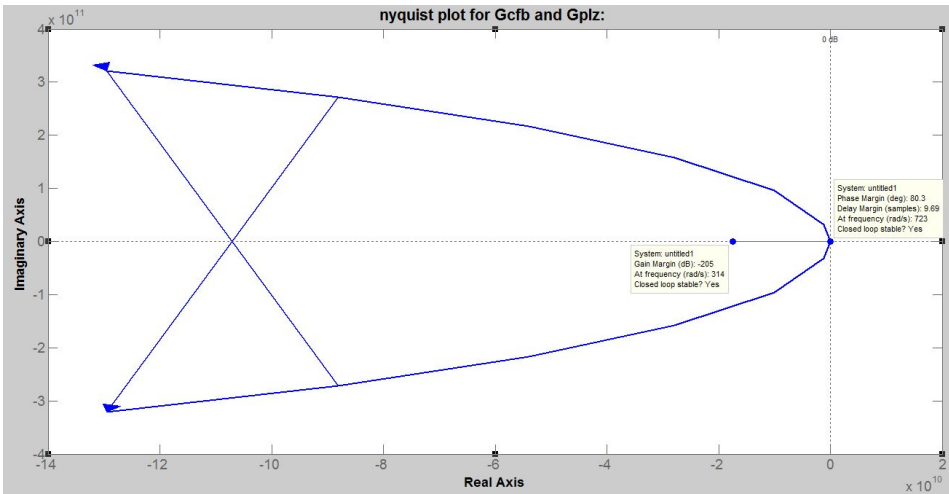


Figure A.14: Nyquist stability plot for case II.

Figures A.14 and A.15 show the stable feature of the current controller via nyquist criterion and frequency stability analysis respectively for the gain parameter set of $K_P=1$ and $K_I=300$ while for the same gain parameter set figure A.16 shows the tracking nature of the current controller via the frequency plot analysis.

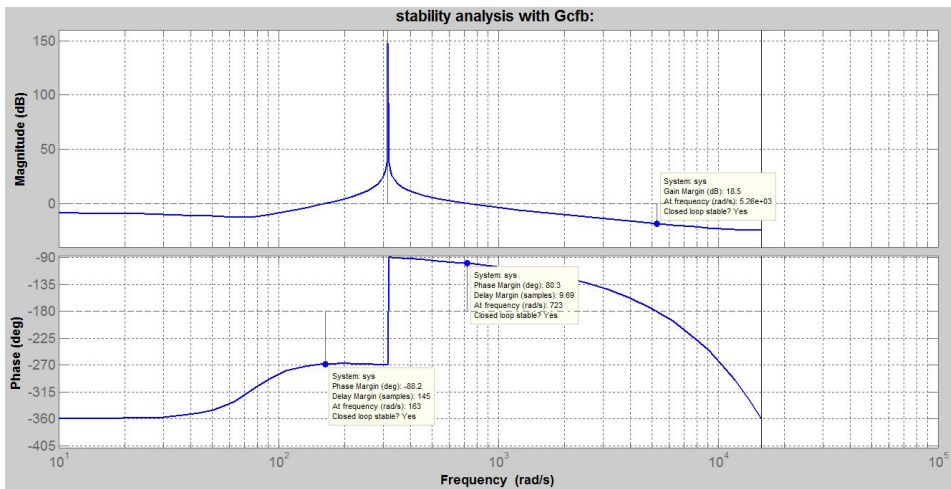


Figure A.15: Frequency stability plot analysis for case II.

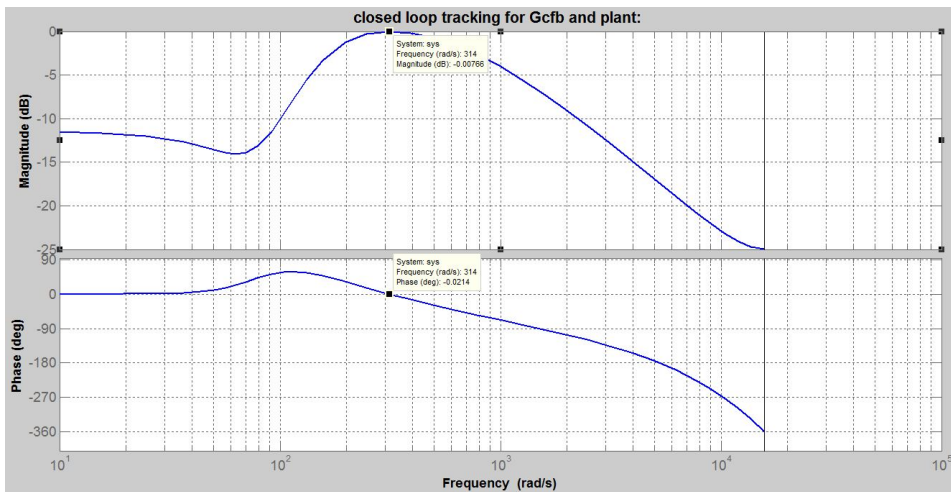


Figure A.16: Tracking nature of the transfer function of the discretized *PR* current controller for case II.

Figures A.17 and A.18 show the stable feature of the voltage controller cascaded with current controller via nyquist criterion and frequency stability analysis respectively for the current controller gain parameter set of $K_P=1$ and $K_I=300$ and the voltage gain parameter set of $K_{P_{hv}}=1$ and $K_{I_{hv}}=200$.

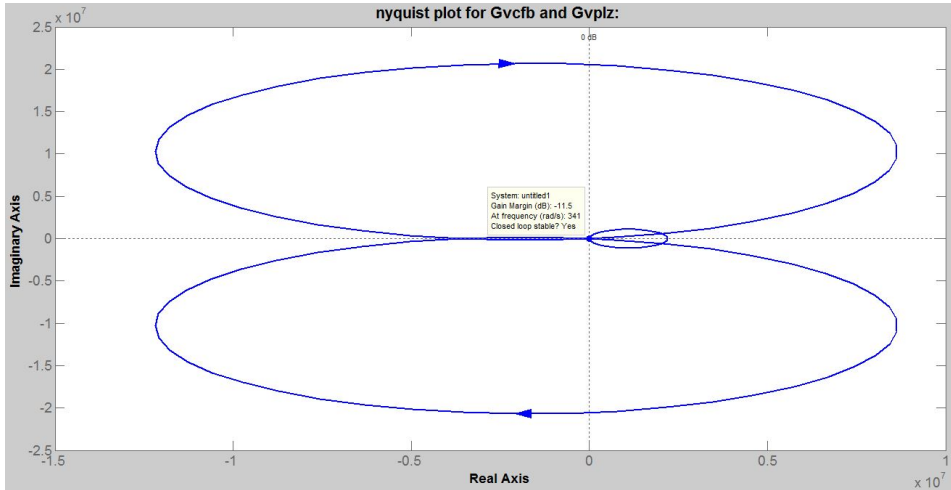


Figure A.17: Nyquist stability plot for cascaded PR voltage controller with PR current controller.

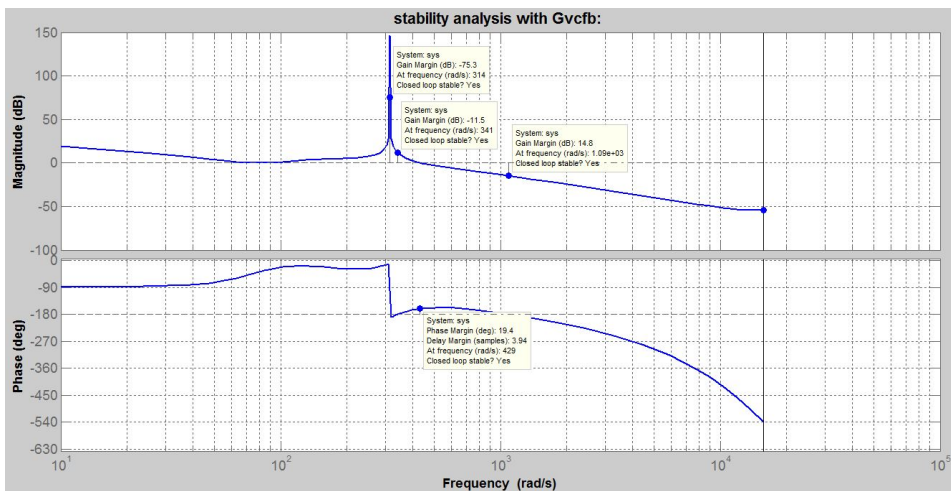
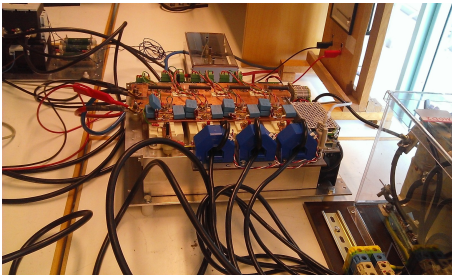


Figure A.18: Frequency stability plot analysis for cascaded PR voltage controller with PR current controller.

A.4 Pictorial Display of the Components used in the Laboratory Setup

The pictures of different elements in the laboratory setup are shown from figures A.19 to A.24.



(a) Converter.



(b) DC voltage side measurement of the converter.

Figure A.19: Converter and the DC voltage side of the converter.

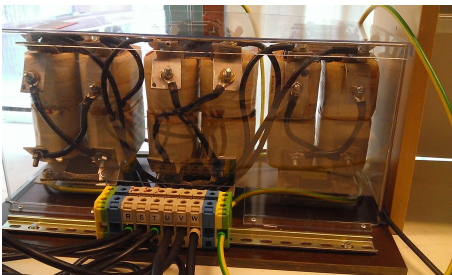


(a) Three sets of three phase contactors on grid converter and load sides.



(b) Grid supply.

Figure A.20: Contactors and the grid supply.

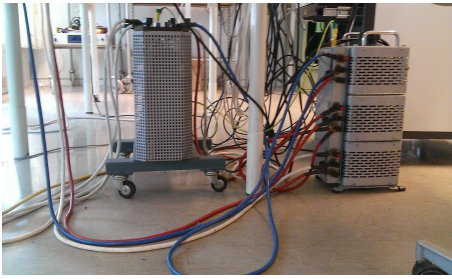


(a) Filter inductors on the converter side.

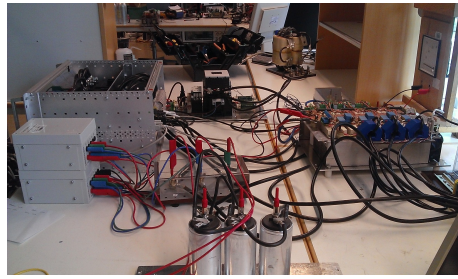


(b) Star connected three phase capacitors of the filter on the converter side.

Figure A.21: Filter elements.

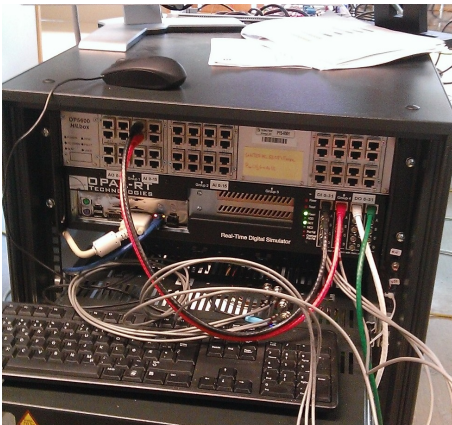


(a) Isolation transformer.



(b) Point of Common Coupling.

Figure A.22: Isolation transformer and PCC.

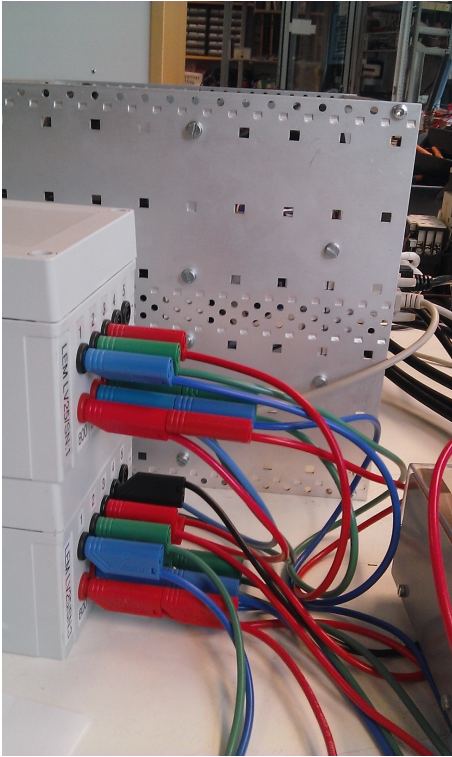


(a) OPAL-RT hardware.



(b) OPAL-RT drives.

Figure A.23: OPAL-RT parts.



(a) Delta connected three phase voltmeters.



(b) Resistive load used.

Figure A.24: Voltmeters and load.

A.5 MATLAB Coding

The MATLAB code below is for the virtual output impedance implementation for PR controllers in continuous domain.

```
1 clear all
2 clc % tuning of the parameters using symmetrical optimum
   method
3 ki=100;
4 kp=1;
5 zeta=0.032;
6 khi=1;
7 prompt = 'What is R?'; %resonant controller gain (20 is
   being used)
8 R= input(prompt);
9 R
10 prompt = 'What is L?'; %resonant controller gain (20 is
   being used)
11 L= input(prompt);L
12 wcHPF=0;
13 Rc=2e-1/0.3187;
14 C=0.3187*990e-6;%capacitance of the filter
15 Td=180e-6;%time delay for the reference current
16 w=2*pi*50;
17 wc=zeta*w;% zeta is the damping ratio being used
18 h0=tf([kp 2*wc*(ki+kp) (kp*w*w)],[1 2*wc w*w]);% it is the
   non ideal PR controller function
19 h0
20 Gpnonidealharmonics=tf([kp 2*wc*(kp+ki) kp*w*w],[1 2*wc w*w
   ]);% it is the non ideal PR controller function%Gf
21 Gpnonidealharmonics
22 Ind=tf([L 0],[1]);
23 Ind
24 Gdelay=tf(1,[Td 1]);% it is the delay function
25 Gdelay
26 Zc=(Rc+tf(1,[C 0]));%it is the capacitive impedance
27 Zc
28 den=(1+(h0*Zc*Gdelay));
29 den
30 Zo=Zc/den;
31 A=Zo*h0*Gdelay;
32 A
33 ZoR=((A*R)+Zo+(A*Ind));
34 ZoR
35 bode((ZoR),{10,1e6});
```

```

36 grid;
37 title('new output impedance with a virtual impedance added
      ');
38 figure;
39 bode(h0/(1+h0),{10,1e6});
40 grid;
41 title('Closed Loop PR Transfer Function ');

```

The MATLAB code below is for the stability and the tracking testing of the discretized PR current and voltage controllers.

```

1  clc;
2  p=180;
3  i=3200;
4  Sn=20e3;%rated apparent power,kVA
5  Vn=200;%peak phase voltage value
6  Vdc=500;%dc voltage value
7  In=sqrt(2)*Sn/(3*Vn/sqrt(2));%peak phase current value
8  Vbase=Vn;
9  Ibase=In;
10 Vdcbase=2*Vbase;
11 kdcpu=Vdc/Vdcbase;
12 fbase=50;%base frequency
13 zbase=Vbase/(Ibase);%base impedance
14 wbase=2*pi*fbase;
15 Lbase=zbase/wbase;
16 Rbase=zbase;
17 Cbase=1/(wbase*zbase);
18 C=990e-6;
19 h=1;
20 w0=wbase;
21 Ts=200e-6;%2e-4;
22 Rf=0.5;
23 Lf=5e-3;
24 Rfpu=Rf/Rbase;%change to pu
25 Lfpu=Lf/Lbase;%change to pu
26 Cpu=C/Cbase;
27 kp=1;%proportional gain for current controller
28 ki=300;%resonant gain for current controller
29 kT=ki*Ts;
30 Ch=((h*w0)^2)-(((h*w0)^4*Ts^2)/12)+(((h*w0)^6*Ts^4)/360);
31 Ch
32 rho=exp(Rfpu*Ts*wbase/Lfpu);
33 rho
34 Gfz=tf([0 (rho-1)/Rfpu],[rho -1],Ts);
35 Gdz=tf([0 1],[1 0],Ts);

```

```

36 Gplz=Gdz*Gfz; % plant function
37 Gplz
38 im=(rho*sin(2*h*w0*Ts))-sin(h*w0*Ts);
39 re=(rho*cos(2*h*w0*Ts))-cos(h*w0*Ts);
40 angleG=-atan(im/re);
41 cc=-2*(1-(Ch*Ts*Ts*0.5));
42 cc
43 phi_h=-angleG;
44 phi_h
45 cos(phi_h)
46 cos((h*w0*Ts)+phi_h)
47 R=tf([cos((h*w0*Ts)+phi_h) -cos(phi_h)],[1 cc 1],Ts);
48 Gcfb=kp+(ki*Ts*R); % PR controller function with delay
    compensation
49 Gcfb
50 q=feedback(Gcfb*Gplz,1);%closed loop representation of
    current controller
51 Gvpcz=tf([0 Ts*wbase/Cpu],[1 -1],Ts);%zero order hold
52 Gvplz=Gvpcz*q;
53 kP=1;
54 kI=200;%25;%15,10;
55 kTv=kI*Ts;
56 Chv=((h*w0)^2)-(((h*w0)^4*Ts^2)/12)+(((h*w0)^6*Ts^4)/360);
57 Chv
58 ccv=-2*(1-(Chv*Ts*Ts*0.5));
59 ccv
60 re_num=(0.008162*cos(2*w0*Ts))-(0.01622*cos(w0*Ts))
    +0.008058;
61 im_num=(0.008162*sin(2*w0*Ts))-(0.01622*sin(w0*Ts));
62 re_den=(1.02*cos(5*w0*Ts))-(4.057*cos(4*w0*Ts))+(6.174*cos
    (3*w0*Ts))-(4.378*cos(2*w0*Ts))+(1.361*cos(w0*Ts))
    -0.1197;
63 im_den=(1.02*sin(5*w0*Ts))-(4.057*sin(4*w0*Ts))+(6.174*sin
    (3*w0*Ts))-(4.378*sin(2*w0*Ts))+(1.361*sin(w0*Ts));
64 anglev=atan(im_num/re_num)-atan(im_den/re_den);
65 phi_hv=-anglev;
66 cos(phi_hv)
67 cos((h*w0*Ts)+phi_hv)
68 Rv=tf([cos((h*w0*Ts)+phi_hv) -cos(phi_hv)],[1 ccv 1],Ts);
69 Gvcfb=kp+(ki*Ts*Rv); % PR controller function with delay
    compensation
70 Gvcfb
71 dbode(Gcfb,{10,1e6},Ts);
72 grid;
73 title('individual characteristics of Gcfb: ');

```

```
74 figure ;
75 dbode(Gvcfb,{10,1e6},Ts);
76 grid;
77 title('individual characteristics of Gvcfb: ');
78 figure;
79 dbode(Gcfb*Gplz,{10,1e6},Ts);
80 grid;
81 title('stability analysis with Gcfb: ');
82 figure;
83 dbode(Gvcfb*Gvplz,{10,1e6},Ts);
84 grid;
85 title('stability analysis with Gvcfb: ');
86 figure;
87 dbode(q,{100,1000},Ts);
88 grid;
89 title('closed loop tracking for Gcfb and plant: ');
90 figure;
91 qv=feedback(Gvcfb*Gvplz,1);
92 dbode(qv,{100,1000},Ts);
93 grid;
94 title('closed loop tracking for Gvcfb and plant: ');
95 figure;
96 nyquist(Gcfb*Gplz);
97 grid;
98 title('nyquist plot for Gcfb and Gplz: ');
99 figure;
100 nyquist(Gvcfb*Gvplz);
101 grid;
102 title('nyquist plot for Gvcfb and Gvplz: ');
103 figure;
```

Appendix **B**

Attached Files

The following files are attached:

- **sdomain_testing.m** - MATLAB code for the virtual output impedance implementation for PR controllers in continuous domain.
- **first_phase_testing.m** - MATLAB code for the stability and the tracking testing of the discretized PR current and voltage controllers.
- **PR_current_controller_only.slx** - Simulink model for case study 1.
- **PR_voltage_and_current_controller.slx** - Simulink model for case study 2.